

DEC 12 1979

not Acc Circ

Q0100

US2

79-1613

c. 2

NBSIR 79-1613

# RADAR ABSORBER MEASUREMENT TECHNIQUES AT FREQUENCIES ABOVE 20 GHz

---

N. S. Nahman  
C. M. Allred  
J. R. Andrews  
C. A. Hoer  
R. A. Lawton

Electromagnetic Technology Division  
National Engineering Laboratory  
National Bureau of Standards  
Boulder, Colorado 80303

Final Report prepared for:  
Department of the Air Force  
Air Force Avionics Laboratory  
Wright-Patterson Air Force Base, Ohio 45433  
Contract MIPR FY117578N2038

August 1979



---

U.S. DEPARTMENT OF COMMERCE, Juanita M. Kreps, Secretary  
Sidney Harman, Under Secretary  
Jordan J. Baruch, Assistant Secretary for Science and Technology  
NATIONAL BUREAU OF STANDARDS, Ernest Ambler, Director

## Table of Contents

	Page
1. INTRODUCTION.....	1
1.1 Review and Perspectives.....	1
1.2 Report Content and Organization.....	2
1.3 References.....	2
2. THE TIME DOMAIN AUTOMATIC NETWORK ANALYZER (TDANA).....	4
2.1 Introduction.....	4
2.2 Extension of Present TDANA Techniques .....	5
2.3 Millimeter Wave Pulse Generator Development.....	7
2.4 Heterodyne Techniques.....	8
2.4.1 Amplitude Modulation - Double Sideband.....	9
2.4.2 Amplitude Modulation - Single Sideband.....	13
2.4.3 Phase Angle Modulation.....	14
2.4.4 Recommendations.....	15
2.5 References.....	15
Figures.....	17
3. IMPROVEMENT OF PICOSECOND-DOMAIN SAMPLING HEADS.....	34
3.1 Introduction.....	34
3.2 Principles of Operation for Sampling (Oscilloscope) Heads.....	34
3.3 Presently Available Devices for Sampling Gates.....	37
3.4 Optically Strobed Sampling Gate .....	37
3.5 Summary.....	37
3.6 References.....	37
Figures.....	39
4. CORRELATION MEASUREMENT SYSTEMS USING NOISE SIGNAL SOURCES.....	43
4.1 Introduction.....	43
4.2 Correlation Functions.....	43
4.3 Using Noise and Correlation Methods for $\mu$ - $\epsilon$ Measurements.....	45
4.3.1 Time Resolution Requirements.....	46
4.3.2 Other Realization Considerations.....	47
4.4 References.....	47
Figures.....	48
5. THE FREQUENCY DOMAIN SIX-PORT AUTOMATIC NETWORK ANALYZER.....	53
5.1 Introduction.....	53
5.2 Theory of the Dual Six-Port Network Analyzer.....	54
5.3 Using Six-Port Systems for $\mu$ - $\epsilon$ Measurements.....	57
5.3.1 The Six-Port Reflectometer.....	57
5.3.2 The Dual Six-Port Network Analyzer.....	57
5.4 References.....	58
Figures.....	59
6. CONCLUSION.....	64
6.1 Summary.....	64
6.2 Discussion.....	64
6.3 Recommendations.....	65

# RADAR ABSORBER MEASUREMENT TECHNIQUES AT FREQUENCIES ABOVE 20 GHz

N. S. Nahman, C. M. Allred, J. R. Andrews

C. A. Hoer and R. A. Lawton

New methods for implementing automatic permittivity/permeability measurements of radar absorber materials for applications primarily above 20 GHz and into the millimeter wave region to about 100 GHz are discussed. A brief review of the state-of-the-art of dielectric and magnetic material measurements is given. Automated time domain and frequency domain methods are considered including time domain automatic network analyzers, correlation measurement systems using noise signal sources, and six-port network analyzers.

Key words: Dielectrics; frequency domain measurements; magnetic materials; microwaves; millimeter waves; permeability measurements; permittivity measurements; radar absorbers; time domain measurements.

## 1. INTRODUCTION

### 1.1 Review and Perspectives

The purpose of this report is to describe new methods for implementing automatic  $\mu$ - $\epsilon$  measurements of radar absorber materials for applications primarily above 20 GHz and into the millimeter wave region to about 100 GHz.

An adequate view of the state-of-the-art for complex  $\mu$  and/or  $\epsilon$  measurements can be obtained from the technical journals; a typical collection of technical papers is given in references [1.1-1.10]. Because of the need to rapidly obtain accurate data for these electromagnetic parameters over broad ranges of frequency and in extreme and changing environments, automated measurement methods are required.

Most of the cited present day techniques are narrowband techniques [1.1-1.6] with the exception of Dispersive Frequency Domain Spectroscopy (DFDS) [1.7,1.8] and Time Domain Spectroscopy (TDS) [1.9,1.10] the latter two techniques employ broadband spectral sources in the form of incoherent and pulsed sources, respectively. DFDS is employed in the optical/infrared regions, while TDS is used in the electrical regions including the higher microwave frequencies.

Regarding terminology, in the electrical region (wavelengths longer than those of the infrared region) noise sources and correlators comprise a system equivalent to the optical/infrared DFDS system. Both systems are based upon correlation functions (observables) and their Fourier transforms. Similarly, TDS is based upon time domain observables and their Fourier transforms. In this case the signal sources are repetitive and of finite duration, and sometimes, periodic.

Recently, new single-frequency measurement techniques based upon six-port or n-port devices have been developed for precision measurements; these techniques are amenable to calibration using fewer standards but require on-line computer data acquisition and processing. However, because of the computer tie-in, the frequency can be rapidly stepped across a frequency band to provide broadband frequency domain measurements. Consequently, such measurement methods could be used to determine complex  $\mu$ - $\epsilon$  data across a broad frequency band.

## 1.2 Report Content and Organization

This report is divided into six chapters, the first one being the present introduction. Four chapters are devoted to time domain spectroscopy, correlation measurement systems with noise signal sources, and frequency domain automatic systems using six-port devices. References appear at the end of each respective chapter. The remaining chapter includes a summary and recommendations for future research and development.

Each of these three new techniques for  $\mu$ - $\epsilon$  measurements are practical techniques. Each one has its own advantages depending upon various considerations. In establishing the feasibility of these new methods, the NBS contributors have developed the analyses presented herein and also have drawn upon their respective experiences in research and development on related measurement techniques in the time domain, correlation, and microwave technical areas. Typical factors such as present measurement capabilities, cost, staff experience, etc., will most probably be the controlling ones for the selection of one method over another. Also, in one frequency band a given technique might be more attractive than another for the very same reasons or combinations of the typical factors cited above. In short, this report does not say which method should be used but does present inclusive recommendations for future technical work. Also, the report provides a technical basis for discussions between the U.S. Air Force (USAF) Avionics Laboratory and NBS.

Chapter 2 is concerned with the time domain automatic network analyzer (TDANA) as applied to  $\mu$ - $\epsilon$  measurements and discusses two topics: (1) extension of present baseband pulse techniques to higher microwave frequencies, and (2) pulsed carrier techniques for microwave/millimeter wave applications. Typical time domain systems are the NBS Automatic Pulse Measurement System (APMS) and the USAF Avionics Laboratory Time Domain  $\mu$ - $\epsilon$  Measurement System.

Because the sampling process and the sampling-head structure fundamentally limit the temporal resolution (and corresponding bandwidth) of sampling oscilloscope systems, improved sampling heads could provide increased temporal resolution. Chapter 3 discusses the improvement of sampling-head hardware using photoconductor gating structures. This concept was invented at NBS under partial support of the USAF. The patent rights have been assigned to the USAF [1.11].

Chapter 4 presents the fundamentals of using noise signal sources for characterizing two-port networks. The desired broadband network or material temporal parameters are extracted by correlation measurements, and the corresponding frequency domain parameters are obtained from the Fourier transforms of the correlation (temporal) functions.

Chapter 5 introduces frequency domain automatic systems, using six-port devices, which are basically single-frequency techniques but are highly amenable to automation and calibration. This, in turn, enables a sequence of rapid measurements to be made over a frequency band.

Finally, Chapter 6 contains a summary of the body of the report's discussion of the major factors involved in implementation of new methods, and recommendations for future technical work.

## 1.3 References

- [1.1] Lynch, A. C., Precise measurements on dielectric and magnetic materials, IEEE Trans. on Instr. and Meas. IM-23, No. 4, 425-431 (Dec. 1974).
- [1.2] Stuchly, S. S., and Stuchly, M. A., A method of permittivity measurement for lossy materials with high dielectric constant, Conference sur Les Mesures Electromagnetiques de Precision, Ottawa, Canada, June 26-29, 1978, pp. 129-130 (CPEM 1978, IEEE Cat. No. 78CH1320-1 IM).
- [1.3] Decreton, M. C., and Gardiol, F. E., Simple nondestructive method for the measurement of complex permittivity, IEEE Trans. on Instr. and Meas. IM-23, No. 4, 434-438 (Dec. 1974).
- [1.4] Hill, G. J., The precise determination of the dielectric properties of alumina, IEEE Trans. on Instr. and Meas. IM-23, No. 4, 443-446 (Dec. 1974).
- [1.5] Meyer, W., High-sensitivity dielectric loss measurements by using superconducting microwave resonators in an oscillator loop, Electronics Letters 13, 7-8 (1977).

- [1.6] Meyer, W., High sensitivity measurement of saturable dielectric loss at cryogenic temperatures, Conference sur Les Mesures Electromagnetiques de Precision, Ottawa, Canada, June 26-29, 1978, pp. 134-136 (CPEM 1978, IEEE Cat. No. 78CH1320-1 IM).
- [1.7] Afsar, M. N., Chamberlain, J., and Chantry, G. W., High precision dielectric measurements on liquids and solids at millimeter and submillimeter wavelengths, IEEE Trans. on Instr. and Meas. IM-25, No. 4, 290-294 (Dec. 1976).
- [1.8] Afsar, M. N., Submillimeter wave measurements on liquid dielectrics, Conference sur Les Mesures Electromagnetiques de precision, Ottawa, Canada, June 26-29, 1978, pp. 131-133 (CPM 1978, IEEE Cat. No. 78CH1320-1 IM).
- [1.9] Cronson, H. M., Nicholson, A. M., Mitchell, P. G., Extensions of time domain metrology above 10 GHz to materials measurements, IEEE Trans. on Instr. and Meas. IM-23, No. 4, 463-468 (Dec. 1974).
- [1.10] Cole, R. H., Time-domain spectroscopy of dielectric materials, IEEE Trans. on Instr. and Meas. IM-25, No. 4, 371-375 (Dec. 1976).
- [1.11] Lawton, R. A., and Andrews, J. R., Waveform sampler, U.S. patent 4 030 840 (June 21, 1977).

## 2. THE TIME DOMAIN AUTOMATIC NETWORK ANALYZER

James R. Andrews

### 2.1 Introduction

Time domain techniques have been applied quite successfully to the measurement of frequency domain parameters at frequencies up to X-band (12 GHz) [2.1-2.10]. These include the complex S-parameters for electrical networks and material parameters [2.4,2.11,2.12] such as the complex permeability and permittivity ( $\mu$  and  $\epsilon$ ) of dielectrics and ferrites. The recent review paper by Andrews summarizes the techniques and state-of-the-art [2.13]. The common features of the time domain automatic network analyzer (TDANA) (fig. 2.1) as used by the various researchers include: (1) a very fast pulse generator, (2) a wideband sampling oscilloscope, and (3) a minicomputer. The USAF Avionics Laboratory  $\mu$ - $\epsilon$  measurement system is an example of such a system [2.14-2.16].

The pulse generators used have typically been either tunnel diode step function generators or step recovery diode (SRD) impulse generators. A step recovery diode generator typically produces a 5 V, 60 ps impulse with a useful spectrum up to 8 GHz. A tunnel diode typically produces a 1/4 V step with a 20 ps transition time and a useful spectrum up to 12 GHz. Recently, measurement capabilities have been extended to the Ku-band (12.4-18 GHz) using improved pulse generators which generate a short rf burst [2.17].

The state-of-the-art in sampling oscilloscopes is "A" which has a 20 ps transition time and a dc to 18 GHz, 3 dB bandwidth.<sup>1</sup> Another sampling oscilloscope often used is the "B". It has a 30 ps transition time and a dc to 11.5 GHz, 3 dB bandwidth.

A minicomputer serves many functions in the operation of a TDANA, including: (1) measurement system controller, (2) data acquisition, (3) data storage, (4) digital averaging to improve signal-to-noise ratio, (5) Fourier transform computation to convert the time data to the frequency domain, (6) computation of the scattering parameters  $S_{ij}$ , or other desired parameters, and (7) presentation of the results in a useful tabular or graphical form to the operator via a cathode ray tube (CRT) terminal.

When one is faced with making S-parameter or  $\mu$ - $\epsilon$  measurements in the millimeter wave region, one question which arises is whether the TDANA technique can be extended to these frequencies. The answer is a qualified "yes." This chapter will deal with this question. The basic TDANA arrangement with a shorter rf pulse burst and the present HP sampler can probably be extended to the K-band (18-26.5 GHz) with some difficulty; the next two sections, 2.2 and 2.3, will address this topic. Above K-band, alternate techniques will no doubt have to be used. At the present time, the most promising appears to be that of heterodyning a baseband pulse up to the millimeter band of interest and then synchronously heterodyning a response signal back to baseband for subsequent measurement; section 2.4 will discuss this topic.

---

<sup>1</sup>In order to avoid influencing the competitive positions of manufacturers of commercial equipment we have not identified these products.

## 2.2 Extension of Present TDANA Techniques

The first question to be faced is, "Will the "A" sampler work at millimeter frequencies?" The manufacturer specifies the transition time to be  $\approx 20$  ps and the bandwidth as dc to greater than 18 GHz. "A-B" and "A-C" samplers owned by NBS do, in fact, have transition times of  $\approx 20$  ps when they are properly adjusted. An NBS Guest Worker, S. M. Riad, as part of his Ph.D. dissertation, mathematically modeled the older "A-A" sampler [18]. The manufacturer specified the bandwidth of the "A-A" to be dc to  $> 12.4$  GHz and the transition time to be  $\approx 28$  ps. Riad's model predicted the step response transition time to be 27.5 ps. Figure 2.2 shows Riad's computed impulse response for the "A-A". The impulse response duration (50%) is 24.1 ps. Figure 2.3 shows the frequency response computed from Riad's impulse response. While it is not mathematically rigorous, an approximation to the "A-B/C" response can be made by scaling figure 2.2 by 20/28 and figure 2.3 by 18/12.4. From this extrapolation, the "A-B/C" amplitude response may be estimated as follows:

Table I. "A-B/C" Predicted Frequency Response

<u>Amplitude Response</u>	<u>Frequency</u>
- 3 dB	18 GHz
- 6 dB	15 GHz
- 10 dB	35 GHz
- 14 dB	42 GHz
- 20 dB	50 GHz

Figure 2.4 is offered as further evidence that the "A-B/C" will function at millimeter frequencies. This figure shows an actual 45 GHz sine wave that was observed on an NBS "A-B" during the development of the SHF impulse generator built for the USAF Avionics Laboratory in 1977 [2.17].

Figures 2.2-2.4 demonstrate that the "A-B/C" sampler will operate above 18 GHz. Because operation is in the high frequency roll-off region, measured waveforms will be considerably distorted. However, when making ratio measurements, such as  $S_{21}$  or  $S_{11}$ , the frequency response effect of the sampler transfer function  $H_S(\omega)$ , will cancel out. In theory,  $H_S(\omega)$  is immaterial in ratio measurements. In practice, it has a significant effect. If  $H_S(\omega)$  is down, then the signal-to-noise ratio in the measurement is reduced and, as a result, the measurement errors are increased.

Although the "A-B/C" sampler response is seen to be useful to at least 50 GHz, there are other problems that present major obstacles to measurements above 18 GHz. They are primarily timing instabilities, such as jitter and long-term drift. The source of these instabilities is in both the sampling oscilloscope time base and the pulse generator. Gans [2.8] and Elliott [2.19] have shown that the effect of signal averaging on a waveform that has time jitter is equivalent to using a low pass filter. For stationary, Gaussian time jitter of standard deviation,  $\sigma_j$ , the filter is of the form

$$H_j(f) \propto e^{-1/2 (2\pi f \sigma_j)^2} \quad (2.1)$$

Table II lists the jitter observed on several different NBS sampling oscilloscopes and pulse generators. These are values representative of the current state-of-the-art. These reported jitter values,  $\tau_j$ , are human observer measurements of the nominal width of the jitter band excluding some outlying samples. They are related to  $\sigma_j$  by

$$\sigma_j \approx 1/2 \tau_j \quad (2.2)$$

The 3 ps value of  $\sigma_j$  reported by Gans [2.8] was obtained from a computer controlled measurement of the complete jitter probability distribution. Also included in Table II is the equivalent filter cutoff frequency (-3 dB) due to the jitter.

Table II. Jitter Characteristics

Sampling Oscilloscope	Pulse Generator	$\tau_j$ (ps)	$f_{co}$ (GHz)
1. "A-B" sampler with "C" time base and "D" vertical amp.	"E" tunnel diode and NBS bias supply	$\tau_j \sim 5-6$ ps (human observation) $\sigma_j = 3$ ps [2.8] (computer meas.)	44
2. "A-B" sampler and "F" sampling plug-in	"E" tunnel diode and NBS bias supply	$\sim 2$ ps (low freq. ripple) $\sim 4$ ps (Gaussian jitter) $\sim 5$ ps (overall)	53
3. "A-B" and "F"	"E" tunnel diode and NBS improved automatic TD bias supply	$\sim 2$ ps (low freq. ripple) $\sim 4$ ps (Gaussian jitter) $\sim 5-6$ ps (overall)	48
4. "A-B" and "F"	"E" tunnel diode and "G" bias supply	$\sim 2$ ps (low freq. ripple) $\sim 5$ ps (Gaussian jitter) $\sim 6-7$ ps (overall)	41
5. "A-B" and "F"	NBS SHF Impulse Generator [2.17]	$\sim 3$ ps (low freq. ripple) $\sim 4$ ps (Gaussian jitter) $\sim 6$ ps (overall)	44
6. "B" sampler with "H" time base and "I" vertical amp.	"E" tunnel diode and NBS improved automatic TD bias supply	$\sim 4$ ps (Gaussian)	66
7. "B", "H" and "I"	NBS SHF Impulse Generator	$\sim 4$ ps (Gaussian)	66

The other major timing error is due to long-term drift (ms or longer). Drifting is potentially more serious than jitter. Drifting has many different causes, including minute temperature fluctuations, line voltage changes, etc. NBS has found it necessary to operate its scopes and generators continuously, to minimize these effects. It is possible to devise special hardware and/or software techniques to minimize these long-term drifts. B. Elliott devised a hardware technique that allowed him to reduce by a factor of 500 the drift of a tunnel diode generator/"A-A" sampler combination [2.20]. The overall drift stability of his system was about 20 fs (0.02 ps). Nicholson developed a hardware/software, 3-point scanning technique to detect and correct drift errors [2.21]. His techniques are used in the present  $\mu$ - $\epsilon$  measurement system at the USAF Avionics Laboratory [2.14]. Both Elliott's and Nicholson's techniques require the use of an additional reference pulse directly related to the signal to be measured. This reference pulse is required to be positioned at a precise location in the time window of observation. These techniques are useful in a TDANA system that is hardwired into a fixed configuration and that is only used for a single type of measurement. To date, these techniques have not been incorporated into the NBS TDANA because it is used for a wide variety of measurements employing many different pulse generators and time windows from 100 ps to several ms.

Another effect that often causes timing problems is the 60 Hz ground currents between the various pieces of equipment. For ps resolution, even minute ground currents can cause noticeable degradation.

To extend the direct measurement performance of the NBS oscilloscope above 18 GHz will require several modifications including: (1) "F-A" time base changes to reduce jitter and 60 Hz interference, (2) system ground loop isolation, and (3) incorporation of hardware/software drift stabilization.

### 2.3 Millimeter Wave Pulse Generator Development

As noted earlier, the present baseband pulse generators used in TDANA's produce a useful spectrum up to 18 GHz. To extend beyond 18 GHz will probably require the use of the same technique used to cover the Ku-band, namely, the generation of a short rf burst. Figure 2.5 shows the waveform and spectrum of an ideal rf burst. The equation for the waveform is

$$v(t) = V_0 [u(t + t_0/2) - u(t - t_0/2)] \sin(2\pi f_c t). \quad (2.3)$$

The spectrum amplitude,  $S(f)$ , is given by

$$S(f) = V_0 t_0 \left| \frac{\sin(\pi \Delta f t_0)}{(\pi \Delta f t_0)} - \frac{\sin[\pi(2f_c + \Delta f)t_0]}{[\pi(2f_c + \Delta f)t_0]} \right| \quad (2.4)$$

where

$$\Delta f = f - f_c. \quad (2.5)$$

Several techniques can be used to generate an rf burst. NBS Tech. Note 699 discusses in detail several of these techniques. One technique is to gate the output of a cw sine wave generator. PIN diode modulators or double balanced mixers can be used as the gates. 2 ns or slower transition times are typical for PIN diodes while 1 ns are typical for double balanced mixers. Another technique that NBS has found useful for generating high power, broadband, microwave rf bursts is to shock-excite a high power, traveling-wave tube amplifier (TWT) with an extremely narrow (< 100 ps) baseband impulse. Figures 2.6 and 2.7 show the waveforms obtained from C-, X-, and Ku-band TWT's. The TWT acts as both a wide bandpass filter (typically octave bandwidths, 2 to 4 GHz, etc.) and a high gain amplifier (30 dB is typical). The output is a short rf burst of a few rf cycles with a frequency near the low end of the TWT passband. Peak power comparable to the output power rating of the TWT can be obtained. As seen in figure 2.7, broadband spectrum amplitudes of the order of 80 dB $\mu$ V/MHz can easily be obtained. The C-band TWT output is useful (20 dB range) from 2 to 13 GHz. The X-band TWT useful range extends from 4 to 15.5 GHz with the exception of a sharp notch at 9.4 GHz. The Ku-band TWT appears to be useful from approximately 10 GHz to 16 GHz.

A second technique for generating a microwave rf burst is to mount a step recovery diode within a piece of waveguide [2.17,2.22]. Figures 2.8 and 2.9 show the waveform and spectrum produced by the SHF impulse generator recently built by NBS for the USAF Avionics Laboratory. The peak-to-peak amplitude is 0.8 V. The center frequency is 12.5 GHz. The 1/e duration is 1/4 ns. The spectrum amplitude is 32 dB $\mu$ V/MHz,  $\pm$  7.5 dB, from 6 to 18 GHz. The step recovery diodes used in the SHF impulse generator were the fastest (60 ps) diodes commercially available. They could also be used in K-band waveguide (RG-53/U) but with reduced output amplitude. If necessary, the amplitude of this rf burst could be increased considerably using a high power TWT.

Techniques other than the step-recovery (snap-off) transition may be more useful at K-band and higher. Other examples are the various types of transferred electron devices such as: avalanche, impatt, trapett, Gunn diodes, etc. Figure 2.4 shown earlier is an example. During the development of the NBS SHF impulse generator, the driving pulse to the waveguide-mounted, step-recovery diode was inadvertently adjusted to exceed the reverse breakdown voltage of the diode. When the diode started conducting in the reverse direction, the 45 GHz oscillations of figure 2.4 were observed. Various solid-state oscillators are now available at frequencies up to at least 200 GHz [2.23]. Extremely fast (< 100 ps) on-off modulation of some of these oscillators should be possible with some modifications. Another idea that should be investigated is the use of a short laser pulse to trigger on an oscillator diode.

## 2.4 Heterodyne Techniques

Heterodyne techniques have been used since the earliest days of wireless. They are a straightforward means of translating from one frequency to another. Heterodyning will permit the extension of baseband pulse measurement techniques to millimeter wavelengths. The baseband spectrum of a test pulse generator can be heterodyned up to a high frequency and passed through an unknown network or material. The response signal can then be downconverted back to baseband for subsequent measurement and analysis. This section will discuss the advantages and disadvantages of various modulation techniques including: amplitude modulation (AM), frequency modulation (FM), phase modulation (PM), and single sideband (SSB). Detection techniques discussed include: amplitude detectors, both linear and square law, frequency discriminator, phase detector, coherent detector, synchronous detector, phase-locked detector, and image rejection mixers.

In general, a modulated signal may be described as

$$v(t) = v_a(t) \sin[\omega(t) t + \phi(t)]. \quad (2.6)$$

In other words, we can modulate either the amplitude [ $v_a(t)$ ], the frequency [ $\omega(t)$ ], or the phase [ $\phi(t)$ ] or any combination of the above. The modulating signal  $v_m(t)$  can be of any form such as periodic, aperiodic, single transient, or random. For the purposes of time domain testing, we will hereafter limit the discussion to periodic signals. The periodic signal may be of any waveshape, including: sine wave, impulse, doublet, rectangular pulse, trapezoidal pulse, rf burst, etc. Being periodic, it can be completely described by a Fourier series expansion of an infinite sum of sines and cosines.

$$v_m(t) = \frac{A_0}{2} + \sum_{n=1}^{\infty} [A_n \cos(2\pi n f_0 t) + B_n \sin(2\pi n f_0 t)] \quad (2.7)$$

where  $f_0$  is the fundamental frequency of the periodic waveform. The frequency coefficients are given by

$$A_n = \frac{2}{T} \int_0^T v_m(t) \cos(2\pi n f_0 t) dt \quad (2.8)$$

$$B_n = \frac{2}{T} \int_0^T v_m(t) \sin(2\pi n f_0 t) dt \quad (2.9)$$

where  $T = 1/f_0$  is the period. The Fourier series can also be written in complex exponential form.

$$v_m(t) = \sum_{n=-\infty}^{+\infty} D_n(n f_0) e^{+j2\pi n f_0 t} \quad (2.10)$$

where

$$D_n = \frac{1}{T} \int_0^T v_m(t) e^{-j2\pi n f_0 t} dt \quad (2.11)$$

$A_n$  and  $B_n$  are real constants while  $D_n$  is a complex constant. Knowing full well that an arbitrary, periodic test signal can be represented by a series of sines and cosines, we will hereafter limit the discussion to a single term in the Fourier series. Additional terms will be added in a real situation but would only serve to confuse the following discussion.

#### 2.4.1 Amplitude Modulation - Double Sideband

Amplitude modulation (AM) can be represented as shown in figure 2.10. This type of modulation may be described by the equations:

$$v_{rf}(t) = k_1 v_m(t) V_c \cos(\omega_c t) \quad (2.12)$$

$$v_m(t) = V_m [1 + m \cos(\omega_m t)] \quad (2.13)$$

where  $m$  is the modulation index and  $k_i$  is the  $i$ th mixer constant ( $i = 1$  for the above).

$$\frac{v_{rf}(t)}{k_1 V_0 V_c} = \cos(\omega_c t) + \frac{m}{2} \cos(\omega_l t) + \frac{m}{2} \cos(\omega_u t) \quad (2.14)$$

$$\omega_l = \omega_c - \omega_m \text{ and } \omega_u = \omega_c + \omega_m .$$

This leads to the classical result with AM that the modulation of a single carrier frequency,  $\omega_c$ , by a single modulation frequency,  $\omega_m$ , creates two sideband frequencies spaced  $\omega_m$  above and below the carrier frequency. The carrier frequency,  $\omega_c$ , term can be considered the same as the dc term. For further Fourier analysis, it can be dropped. Actually, if a double balanced mixer is used, the dc component of the modulation is removed, and  $m$  is set to 1, then the carrier will be suppressed and the output will only consist of two sidebands (DSB). Thus eq (2.14) becomes:

$$v_{rf}(t) = k_1 V_m \cos(\omega_m t) V_c \cos(\omega_c t) \quad (2.15)$$

$$v_{rf}(t) = k_1 \frac{V_m V_c}{2} [\cos(\omega_l t) + \cos(\omega_u t)] \quad (2.16)$$

If the rf test signal is then passed through an unknown network,  $H(\omega)$ , the output is given by

$$V_o(\omega) = H(\omega) V_{rf}(\omega). \quad (2.17)$$

In general, the network transfer function is frequency dependent and is not symmetrical about  $\omega_c$ . Although we are concerned with measuring networks or materials, this same problem arises in short-wave radio communication. There, the ionosphere creates selective fading which can cause severe distortion of the received signal. In general, the relative amplitudes and phases of the two sidebands will be altered, but not in the same way for each sideband. Thus, the output equation must reflect this effect.

$$v_o(t) = \frac{k_1 V_m V_c}{2} [H_l \cos(\omega_l t + \phi_l) + H_u \cos(\omega_u t + \phi_u)] \quad (2.18)$$

After some mathematical manipulation, this can be expressed in the form

$$v_o(t) = \frac{k_1 V_m V_c}{2} H_{u\ell m} \operatorname{Re} [ e^{j\psi_{u\ell m}} e^{j\omega_m t} e^{j\omega_c t} ] \quad (2.19)$$

where

$$H_{u\ell m} = [(H_u \cos \phi_u - H_l \cos \phi_l)^2 + (H_u \sin \phi_u + H_l \sin \phi_l)^2]^{1/2} \quad (2.20)$$

and

$$\psi_{u\ell m} = \tan^{-1} \left[ \frac{H_u \sin \phi_u + H_l \sin \phi_l}{H_u \cos \phi_u - H_l \cos \phi_l} \right] \quad (2.21)$$

An important conclusion to note from the above is that in general we have two measurable quantities, namely  $H_{u\ell m}$  and  $\psi_{u\ell m}$ , but they are functions of four unknown variables, namely,  $H_u$ ,  $\phi_u$ ,  $H_l$ , and  $\phi_l$ .

The next question that needs to be addressed is the detection of the rf signal. The simplest technique is the diode envelope detector (fig. 2.11). The diode detector's output is proportional only to the envelope amplitude of the rf signal.

$$v_d(t) \propto |V_{rf}|^p \quad (2.22)$$

A nonlinear element, typically a semiconductor diode, is used to perform the detection process. For large signal levels, the diode output is linear ( $p = 1$ ). For low level signals, the detected output typically follows the square law ( $p = 2$ ). However, in practice, neither the truly linear nor the square law detector is really achieved. With a proper choice of input level and circuit constants, the ideal conditions can be approached closely.

The AM (DSB) signal involves four unknowns, and the simple diode detector gives only one measurable parameter. Thus the use of AM (or DSB) and a diode detector is not the proper choice for rf heterodyne network measurements.

The synchronous detector (fig. 2.12) is a detection scheme that permits the measurement of both the amplitude and phase of an rf signal. Examination of figure 2.12 shows that a synchronous detector is simply a heterodyne mixer fed with a local oscillator identical in frequency to the incoming rf signal. For the situation shown in figure 2.12, the detector output,  $v_{sd}$ , is

$$v_{sd}(t) = k_2 v_o(t) V_{lo} \cos(\omega_c t) \quad (2.23)$$

When eq (2.18) is used for  $v_o(t)$ ,  $v_{sd}$  is found to contain terms at frequencies  $\omega_m$  and  $2\omega_c \pm \omega_m$ . The low pass filter rejects the  $2\omega_c \pm \omega_m$  terms with the result that  $v_{sd}$  is given by

$$v_{sd}(t) = \frac{k_1 k_2 V_m V_c V_{lo}}{4} [H_u \cos(\omega_m t + \phi_u) + H_l \cos(\omega_m t - \phi_l)] \quad (2.24)$$

Thus, the amplitude and phase information of  $H_u$  have been directly translated from rf frequencies to baseband frequencies. From eq (2.24) we can write two equations (amplitude and phase of the modulation frequency,  $\omega_m$ ), but they still involve four unknowns,  $H_l$ ,  $\phi_l$ ,  $H_u$ , and  $\phi_u$ .

What is really needed is some technique for selectively removing one of the sidebands and then measuring the network response to the remaining sideband. This could be done by brute force filtering of the generated DSB signal. However, the requirements imposed on the filter would be quite stringent. Also, new filters would be required each time one wished to move the carrier frequency.

Another technique that can be used to separate the information from the two sidebands is to deal with the quadrature nature of a DSB signal. Consider again the DSB case described earlier in eqs (2.15-2.18). Equation (2.18) can be rewritten in the form

$$v_o(t) = v_i(t) \cos(\omega_c t) - v_q(t) \sin(\omega_c t). \quad (2.25)$$

$v_i(t)$  and  $v_q(t)$  are the "in-phase" and "quadrature" components, respectively, of  $v_o(t)$ . They are given by

$$v_i(t) = \frac{k_1 V_m V_c}{2} [H_u \cos(\omega_m t + \phi_u) + H_l \cos(\omega_m t - \phi_l)] \quad (2.26)$$

$$v_q(t) = \frac{k_1 V_m V_c}{2} [H_u \sin(\omega_m t + \phi_u) - H_l \sin(\omega_m t - \phi_l)]. \quad (2.27)$$

$v_i$  and  $v_q$  can be detected independently if two synchronous detectors are used as shown in figure 2.13. Note that the LO phase for the quadrature detector is shifted by 90°. The in-phase detector is the same as shown in figure 2.12 and described by eqs (2.23) and (2.24).  $v_{id}(t)$  is  $v_{sd}(t)$  as given by eq (2.24).

$$v_{id}(t) = 1/2 k_2 V_{lo} v_i(t). \quad (2.28)$$

The quadrature detector output is given by

$$v_{qd}(t) = v_o(t) k_3 V_{lo} [-\sin(\omega_c t)]. \quad (2.29)$$

After the  $2\omega_c$  terms are filtered out, this reduces to

$$v_{qd}(t) = 1/2 k_3 V_{lo} v_q(t). \quad (2.30)$$

We now have two waveforms from which we can measure two separate magnitudes and phases. All that remains is to find a mathematical separation to extract the four unknowns ( $H_l$ ,  $\phi_l$ ,  $H_u$ , and  $\phi_u$ ) from  $v_{id}$  and  $v_{qd}(t)$ .

The Hilbert transform [2.24,2.25] provides the key to unlocking the puzzle. The Hilbert transform  $\hat{x}(t)$  of a signal  $x(t)$  is given by the principal value of the following equation:

$$\hat{x}(t) = H[x(t)] = \frac{1}{\pi} \int_{-\infty}^{\infty} \frac{x(\tau)}{t-\tau} d\tau. \quad (2.31)$$

$\hat{x}(t)$  is the convolution of  $x(t)$  with  $1/t$ . The Hilbert transform can be thought of as a network that phase-shifts the positive frequencies by  $-90^\circ$  and the negative, by  $90^\circ$ . The Fourier transform of  $\hat{x}(t)$  is  $\hat{X}(f)$  and is related to  $x(t)$  and  $X(f)$  by

$$\hat{X}(F) = -j(\text{sgn } f) X(f). \quad (2.32)$$

For example, if

$$x(t) = \cos(\omega t), \text{ then } \hat{x}(t) = \sin(\omega t) \quad (2.33)$$

or if

$$x(t) = \sin(\omega t), \text{ then } \hat{x}(t) = -\cos(\omega t). \quad (2.34)$$

Applying these results to the detected i and q signals, we can write  $v_{qd}(t)$  as

$$\hat{v}_{qd}(t) = H[v_{qd}(t)] = \frac{1}{4} k_1 k_3 V_m V_c V_{\ell 0} [-H_u \cos(\omega_m t + \phi_u) + H_\ell \cos(\omega_m t - \phi_\ell)]. \quad (2.35)$$

If the two detector mixers are identical

$$k_2 = k_3 = k_d \quad (2.36)$$

then the sums and differences  $v_{id} \pm \hat{v}_{qd}$  will give the separated lower and upper sideband components.

$$v_{\ell d}(t) = v_{id}(t) + \hat{v}_{qd}(t) = \left( \frac{1}{2} k_1 k_d V_m V_c V_{\ell 0} \right) H_\ell \cos(\omega_m t - \phi_\ell) \quad (2.37)$$

$$v_{ud}(t) = v_{id}(t) - \hat{v}_{qd}(t) = \left( \frac{1}{2} k_1 k_d V_m V_c V_{\ell 0} \right) H_u \cos(\omega_m t + \phi_u) \quad (2.38)$$

Equations (2.37) and (2.38) were the sought for results. They show that we can use DSB if we use an I and Q synchronous detector and further process the quadrature component using the Hilbert transform.  $v_{id}(t)$  and  $v_{qd}(t)$  can be measured directly by a TDANA sampling oscilloscope. Then, the Hilbert transform,  $\hat{v}_{qd}(t)$ , and the sums and differences  $v_{id}(t) \pm \hat{v}_{qd}(t)$  can be performed by the TDANA minicomputer. It is also possible to perform these operations in an analog fashion using quadrature hybrids and power dividers/combiners. An I and Q synchronous detector with these additional components is called an image rejection mixer [2.26].

The envelope function,  $v_{ed}$ , can also be expressed in terms of the I & Q components.

$$v_{ed}(t) = (v_{id}^2 + v_{qd}^2)^{1/2} \quad (2.39)$$

Figure 2.14 shows a proposed heterodyne TDANA. It uses DSB signal generation and synchronous I and Q detection. The minicomputer is used to perform the necessary Hilbert transform. The major

bandwidth limitation in this scheme is the available i-f bandwidth of the double balanced microwave mixers. DC to 4 GHz appears to be the state-of-the-art at present [2.26]. With this setup, a single TDANA measurement will yield data over an 8 GHz frequency span ( $f_c \pm 4$  GHz). If a 10 ns time window is used, then the frequency spacing of the resultant data would be 100 MHz.

#### 2.4.2 Amplitude Modulation - Single Sideband

As well as using DSB, one should also consider using single sideband (SSB). The brute force filtering technique of SSB generation was mentioned earlier and dismissed as impractical for this application. SSB can also be generated using the phasing technique [2.24-2.29]. It is more adaptable to the requirement of moving the carrier frequency. Figure 2.15 shows a block diagram for a phasing SSB generator. The output of modulator A is

$$v_{ao}(t) = kV_m \cos(\omega_m t) V_c \cos(\omega_c t). \quad (2.40)$$

Modulator B is assumed to be identical to A, and its output is given by

$$v_{bo}(t) = kV_m \cos(\omega_m t - \pi/2) V_c \cos(\omega_c t - \pi/2) \quad (2.41)$$

The output of the summer is the lower sideband.

$$v_{lsb}(t) = v_{ao}(t) + v_{bo}(t) = kV_c V_m \cos[(\omega_c - \omega_m)t]. \quad (2.42)$$

If one of the 90° phase shift networks is moved to modulator A, then one obtains the upper sideband.

$$v_{usb}(t) = kV_c V_m \sin[(\omega_c + \omega_m)t]. \quad (2.43)$$

The above results, however, are purely theoretical. In practice, one never achieves perfect sideband suppression due to slight variations in the various components used. The most difficult parameters to maintain are the 90° phase shift networks. Pappenfus [2.27] has derived formulas for the sideband suppression as a function of the amplitude and phase imbalance. 0.5° imbalance in either the carrier or modulation will result in 47 dB sideband suppression. 2° gives 35 dB and 5° gives 27 dB. Likewise, 0.1 dB amplitude imbalance results in 46 dB sideband suppression. 0.5 dB gives 31 dB and 1.0 dB gives 25 dB. Imperfect sideband suppression directly introduces errors into any heterodyne measurements. They become particularly serious when measuring a network with a sharp cutoff, such as a bandpass filter.

To receive the SSB signal and downconvert it to baseband, a synchronous detector should be used. If an image rejection mixer is used, additional suppression of the unwanted sideband is obtained. The image rejection mixer is simply another phasing SSB generator operated in reverse.

Figure 2.16 shows a proposed SSB TDANA. For the purposes of broadband TDANA measurements, it is desirable to use a baseband frequency range that is as wide as possible. There are several conflicting requirements, however. The major one is the bandwidth of the 90° phase shift networks. Most quadrature (90°) hybrids typically have a bandwidth of one octave. There are some broadband quadrature hybrids that span several octaves, but their phase and amplitude specifications are rather loose. Another consideration is the i-f bandwidth of the double balanced mixers (DBM). Most DBM's typically have i-f bandwidths of dc up to 1 GHz. Some are available with i-f bandwidths up to 4 GHz. In light of these factors and the sampling oscilloscope and pulse generator limitations, it appears that an i-f frequency of 1 to 4 GHz would be optimum. Baseband frequencies less than 1 GHz will have to be sacrificed in this arrangement due to the poor low frequency performance of the quadrature hybrids. With this setup, a single TDANA measurement would yield data over a 3 GHz frequency span. Again, if a 10 ns time window is used, the frequency spacing of the resultant data would be 100 MHz.

Figures 2.14 and 2.16 are two proposed heterodyne TDANA's. It is not clear at this time which system will give superior results. Additional study will be required before a conclusion can be reached. It is also possible that a hybrid system may offer additional advantages. The hybrid would consist of an SSB generator and the synchronous I and Q detectors with minicomputer Hilbert transformation.

### 2.4.3 Phase Angle Modulation

So far in this section we have only discussed various forms of amplitude modulation. The other important modulation technique is angle modulation, either frequency modulation (FM) or phase modulation (PM). There is essentially no difference between FM and PM because the instantaneous frequency  $\omega_i$  is the derivative of the phase.

$$\omega_i = \frac{d\phi}{dt} \quad (2.44)$$

or conversely, the phase is the integral of the frequency

$$\phi = \int \omega_i dt \quad (2.45)$$

Phase modulation can be represented as shown in figure 2.17 for the elementary case of single-tone modulation.

$$v_{pm}(t) = V_c \cos[\omega_c t + \phi_m(t)] \quad (2.46)$$

$$\phi_m(t) = \phi_d \sin(\omega_m t). \quad (2.47)$$

$\phi_d$  is the modulation index. For this simple case

$$v_{pm}(t) = V_c \cos[\omega_c t + \phi_d \sin(\omega_m t)] \quad (2.48)$$

It is easily shown [2.25, also 2.24, 2.28, and 2.29] that  $v_{pm}(t)$  is periodic and may be expressed in a Fourier series as

$$v_{pm}(t) = V_c \sum_{n=-\infty}^{\infty} J_n(\phi_d) \cos[(\omega_c + n\omega_m)t]. \quad (2.49)$$

This function  $J_n(\phi_d)$  is the  $n$ th order Bessel function of the first kind.

Thus in sharp contrast to the AM case where single tone modulation created two sideband frequencies, PM (or FM) creates an infinite number of sideband frequencies. In actual practice, the Bessel functions are damped out for large arguments so that there are only a finite number of significant sidebands. Nevertheless, if we attempt to measure an unknown network or material with a PM or FM test signal, we end up receiving a response signal with many more unknowns than we have measurable quantities.

The effects of the transmission of a PM or FM signal through a linear network have been mathematically analyzed [2.24]. Complete but extremely involved solutions can be obtained which require computer calculation. Approximations can be made using the "quasistationary" method [2.24]. Extreme care must be exercised in the use of this method because divergent series are the typical output. It is most useful when the transmission characteristics vary in a simple manner.

Brown has used PM in a TDANA to measure the characteristics of millimeter waveguides [2.30]. However, it is the opinion of this author that PM and FM are not valid modulation techniques for performing heterodyned TDANA measurements. This is due to the infinite number of sideband frequencies associated with PM and FM. This does not mean that PM and FM are of no value. They are extremely useful modulation techniques for communication purposes.

#### 2.4.4 Recommendations

It is the recommendation of this author that the most promising technique for TDANA measurements in the millimeter wave region is the pulse heterodyne method. The differences between DSB with I and Q synchronous detectors and SSB with an image rejection mixer need further detailed study.

#### 2.5 References

- [2.1] Nicholson, A. M., Broadband microwave transmission characteristics from a single measurement of the transient response, IEEE Trans. Instr. Meas. IM-17, 395-402 (Dec. 1968).
- [2.2] Ross, G. F., and Nicholson, A. M., The measurement of the intrinsic properties of materials by time domain techniques, IEEE Trans. Instr. Meas. IM-19, 377-382 (Nov. 1970).
- [2.3] Nicholson, A. M., et al., Applications of time domain metrology to the automation of broadband microwave measurements, IEEE Trans. Microwave Theory Tech. MTT-20, 3-9 (Jan. 1972).
- [2.4.] Cronson, H. M., and Ross, G. F., Current status of time domain metrology in material and distributed network research, IEEE Trans. Instr. Meas. IM-19, 495-500 (Nov. 1972).
- [2.5] Cronson, H. M., and Mitchell, P. G., Time domain measurements of microwave components, IEEE Trans. Instr. Meas. IM-20, 320-325 (Nov. 1973).
- [2.6] Bancroft, J., and Johnston, R., Microwave measurements by Fourier analysis of network pulse response, Proc. IEEE 61, 472-473 (April 1973).
- [2.7] Hannaford, D., The application of picosecond pulses in time domain metrology, Proc. 1974 Joint Measurement Conf. (NBS, Gaithersburg, MD, Nov. 12-14, 1974).
- [2.8] Gans, W. L., and Andrews, J. R., Time domain network analyzer for measurement of rf and microwave components, NBS Tech. Note 672, NBS Boulder, CO (Sept. 1975).
- [2.9] Andrews, J. R., and Gans, W. L., Time domain automatic network analyzer, L'Onde Electrique Paris, France, Vol. 55, No. 10, pp. 569-574 (Oct. 1975).
- [2.10] Gans, W. L., Present capabilities of the NBS automatic pulse measurement system, IEEE Trans. Instr. Meas. IM-25, No. 4, 384-388 (Dec. 1976).
- [2.11] Krueger, C. H., and Carter, L. E., Measurement of the high temperature electrical properties of ferrites using time domain techniques, Conference Precision Electromagnetic Measurements (London, 1974).
- [2.12] Cronson, H. M., et al., Extensions of time domain metrology above 10 GHz to materials measurements, IEEE Trans. Instr. Meas. IM-21, 463-468 (Dec. 1974).
- [2.13] Andrews, J. R., Automatic network measurements in the time domain, Proc. IEEE 66, No. 4, 414-423 (April 1978).
- [2.14] Nicholson, A. M., et al., Time domain measurement of microwave absorbers, AF Tech. Report, AFAL-TR-71-353 (Nov. 1971).
- [2.15] Cronson, H. M., and Mitchell, P. G., Time domain measurement system, AF Tech. Report AFAL-TR-72-353 (Dec. 1972).
- [2.16] Nicholson, A. M., et al., Time domain measurement of microwave absorbers 9-16 GHz frequency band, AF Tech. Report, AFAL-TR-73-435 (April 1974).

- [2.17] Andrews, J. R., and Baldwin, E. E., SHF impulse generator, NBSIR 78-888, NBS, Boulder, CO (June 1978).
- [2.18] Riad, S. M., and Nahman, N. S., Applications of the homorphic transformation to time domain measurement problems, NBSIR 78-881, NBS, Boulder, CO (June 1978).
- [2.19] Elliott, B. J., System for precise observation of repetitive picosecond pulse waveforms, IEEE Trans. Instr. and Meas. IM-19, No. 4, 391-395 (Nov. 1970).
- [2.20] Elliott, B. J., High-sensitivity picosecond time domain reflectometry, IEEE Trans. Instr. and Meas. IM-25, No. 4, 376-379 (Dec. 1976).
- [2.21] Nicholson, A. M., Wideband system function analyzer employing time to frequency domain translation, WESCON, Session 22 (San Francisco, Aug. 1969).
- [2.22] Nicholson, A. M., et al., Subnanosecond risetime pulse generators, IEEE Trans. Instr. and Meas. IM-25, 104-107 (June 1976).
- [2.23] Kramer, N. B., Solid-state technology for millimeter waves, Microwave Journal, 57-61 (Aug. 1978).
- [2.24] Schwartz, M., Bennett, W. R., and Stein, S., Communication Systems and Techniques (McGraw Hill, New York, Chapter 1, 1966).
- [2.25] Sakrison, D. J., Communication Theory: Transmission of Waveforms and Digital Information (J. Wiley and Sons, New York, Chapter 5, 1968).
- [2.26] Anaren Microwave, Inc., Catalog, Publication M9001-67 (Syracuse, New York, 175-178, 1976).
- [2.27] Pappenfus, E. W., Bruene, W. B., and Schoenike, E. O., Single Sideband Principles and Circuits (McGraw-Hill, New York, Chapter 4, 1964).
- [2.28] Black, H. S., Modulation Theory (Van Nostrand, Co., New York, Chapter 10, 1953).
- [2.29] Carlson, A. B., Communication Systems - An Introduction to Signals and Noise in Electrical Communication (McGraw-Hill, New York, 2nd Edition, 1968).
- [2.30] Brown, R. J., and Brostrup-Jensen, P., Application of time-domain techniques for measurement and equalization of a millimeter-waveguide line in the 40 to 110 GHz band, IEEE Trans. Instr. and Meas. IM-25, 392-397 (Dec. 1976).

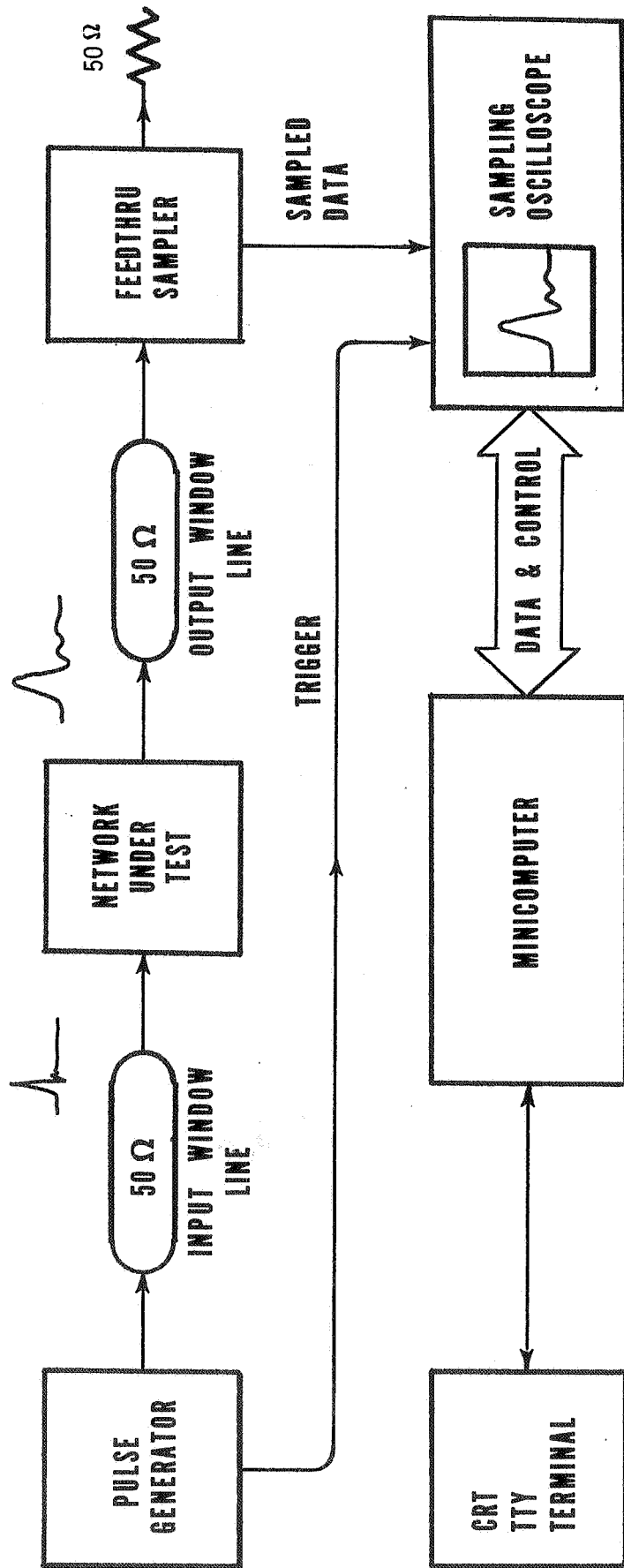


Figure 2.1 TDANA configuration for  $S_{21}$  measurement. For  $S_{11}$  the relative positions of the network under test and the sampler are interchanged.

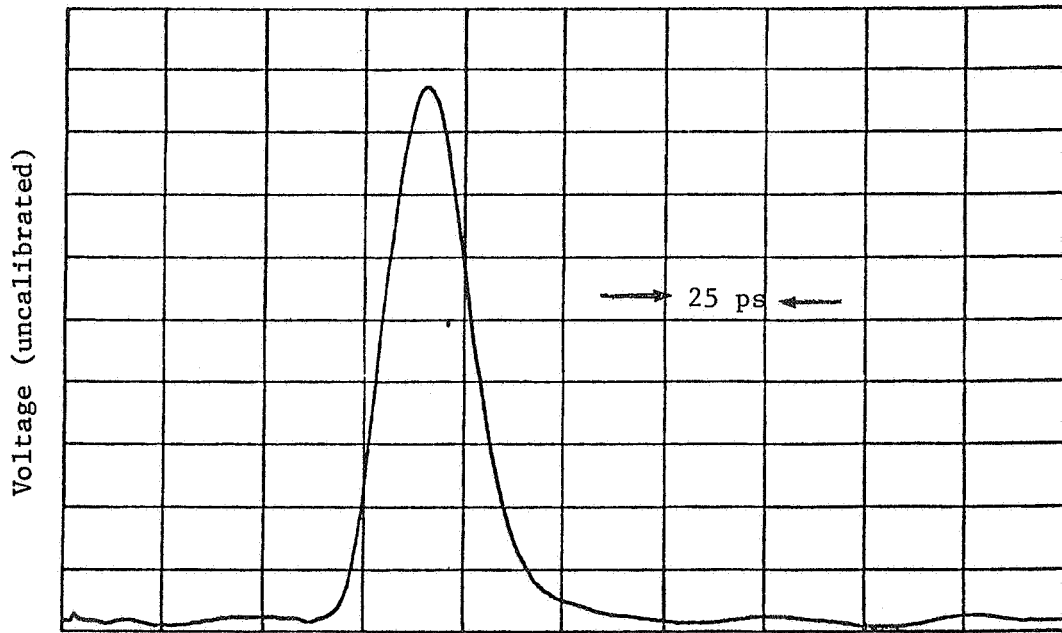


Figure 2.2. Riad's computed impulse response of the "A-A" Sampler.

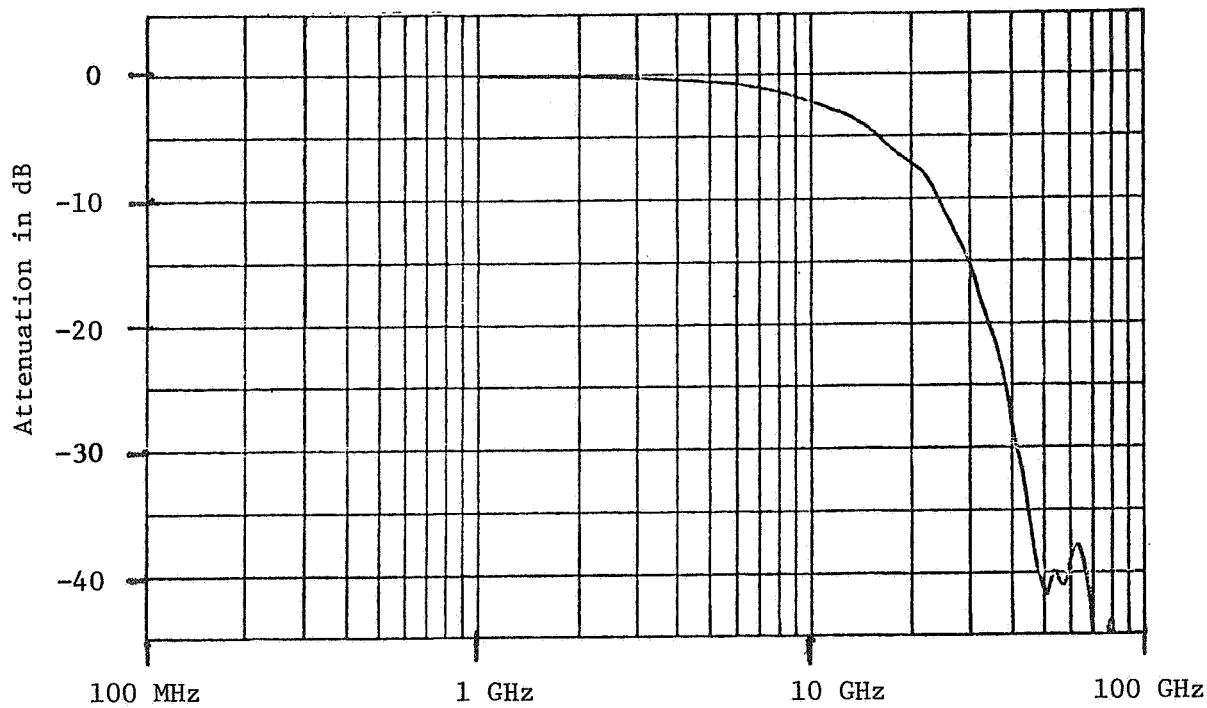


Figure 2.3. Riad's computed frequency response of the "A-A" Sampler.

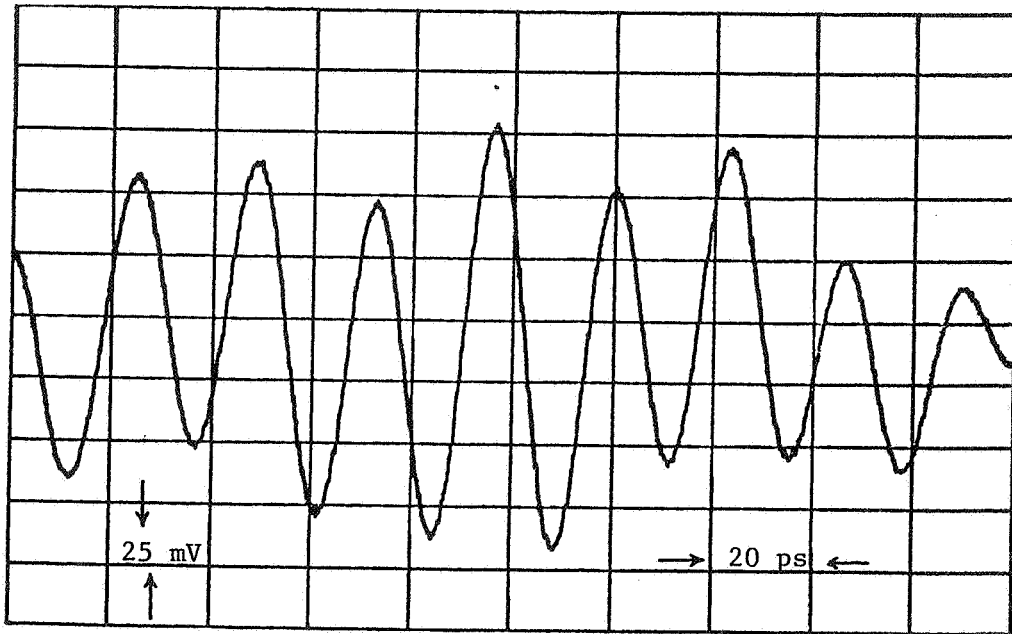


Figure 2.4. 45 GHz sine wave observed on an "A-B" sampler.

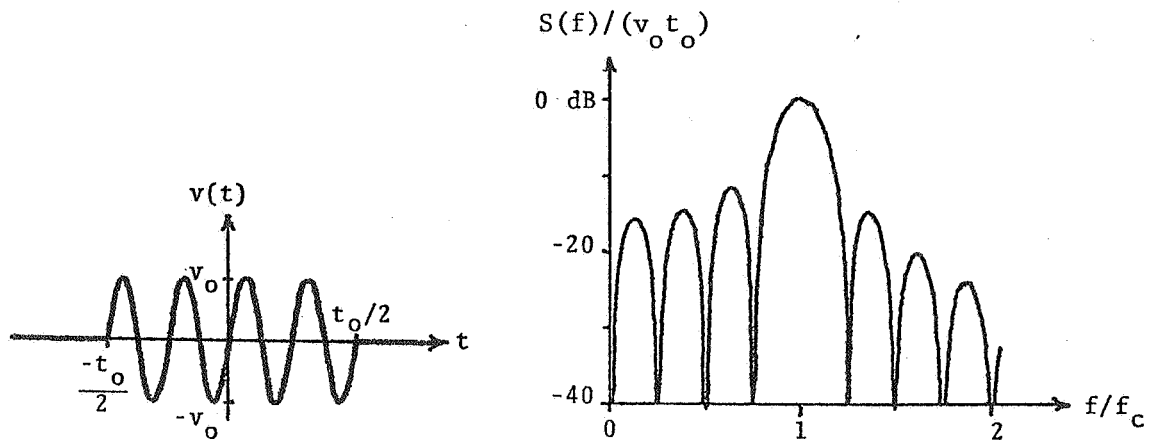
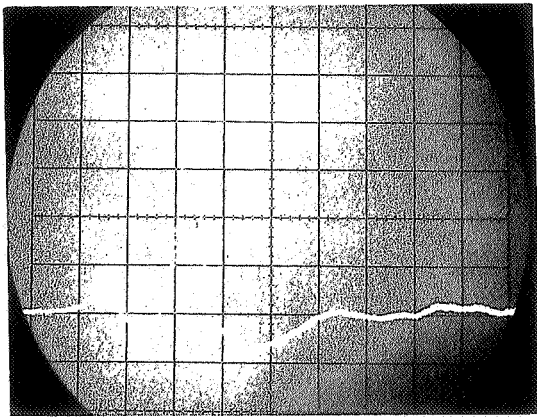
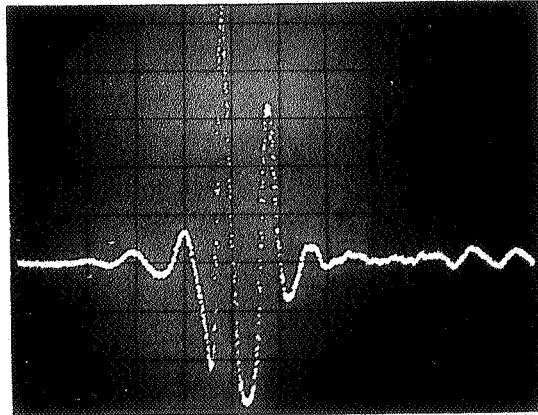


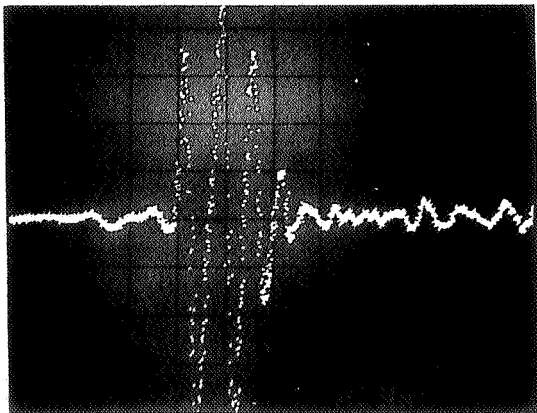
Figure 2.5. Waveform and spectrum of an ideal RF burst.



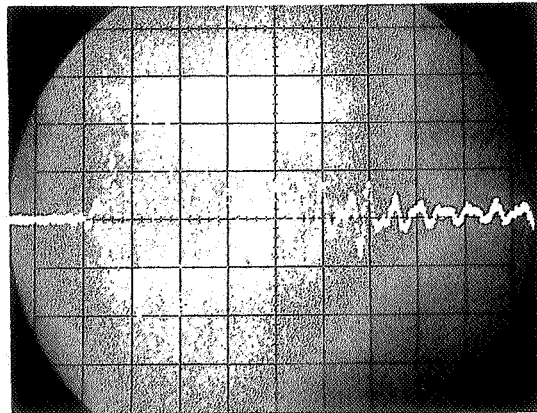
(a)



(b)



(c)



(d)

Figure 2.6. Impulse response of TWTAs. Vertical: 10 V/div. except (a) which is 3.2 V/div. Horizontal: 200 ps div. (a) NBS SRD impulse generator (SN 3-75-3) used as input to TWTA. (b) C band, 30 dB, 10 W TWTA. Input impulse attenuated 15 dB. (c) X band, 30 dB, 20 W TWTA. Input impulse attenuated 16 dB. (d) Ku band, 30 dB, 20 W TWTA.

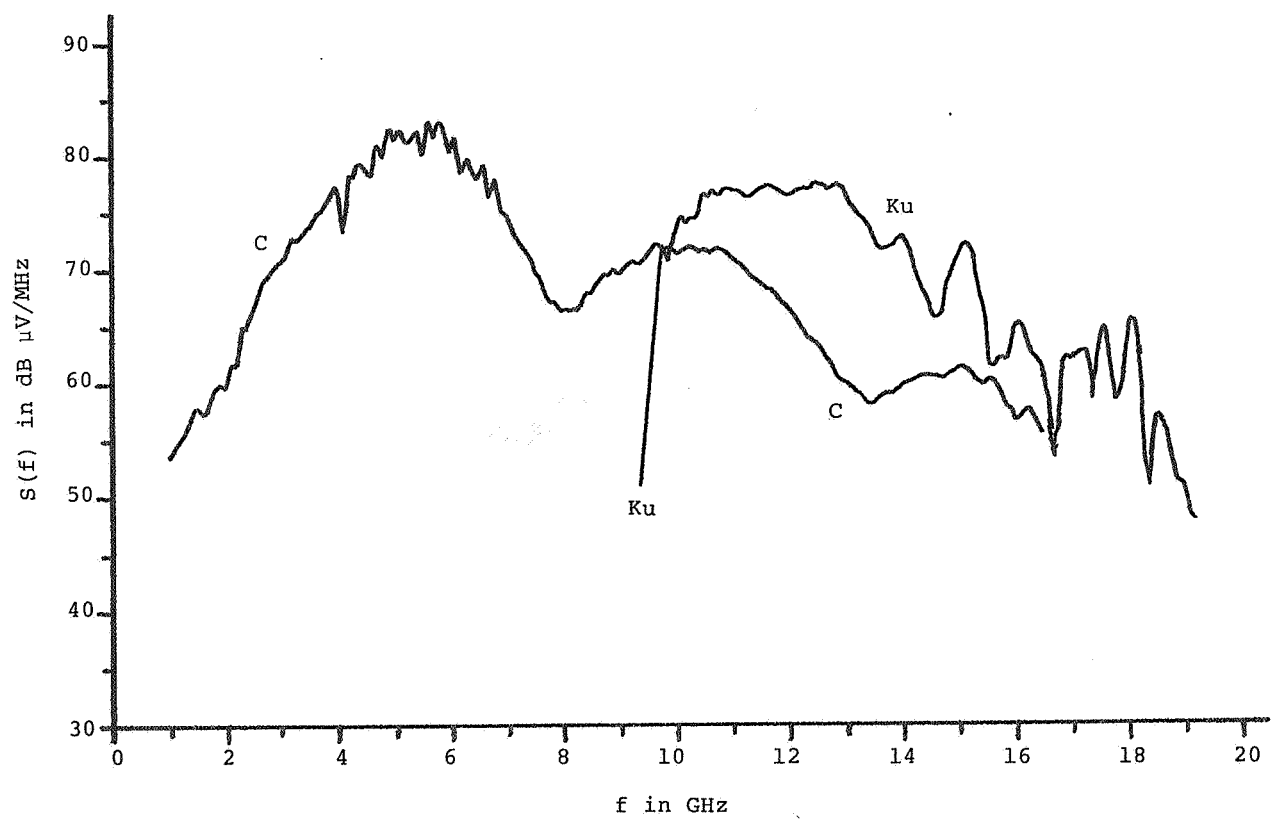
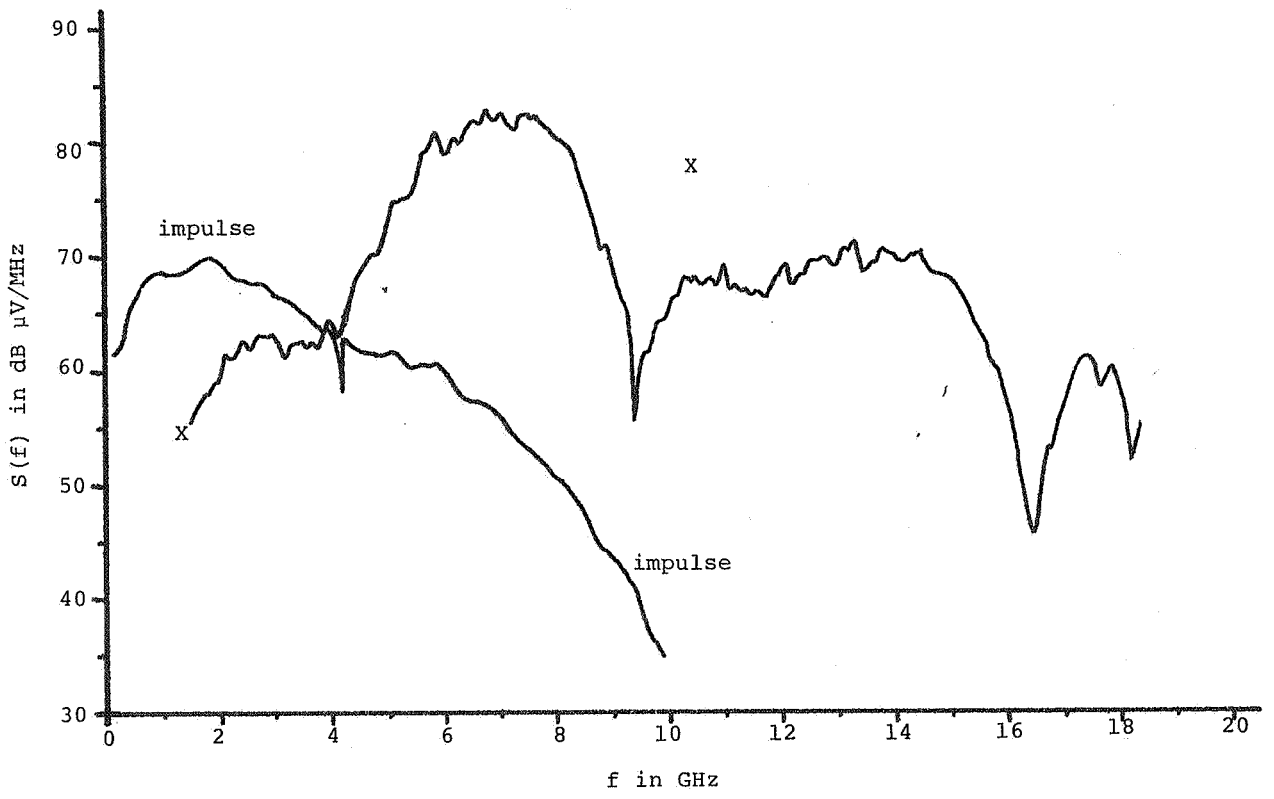


Figure 2.7. Spectrum amplitudes of TWTA impulse responses.

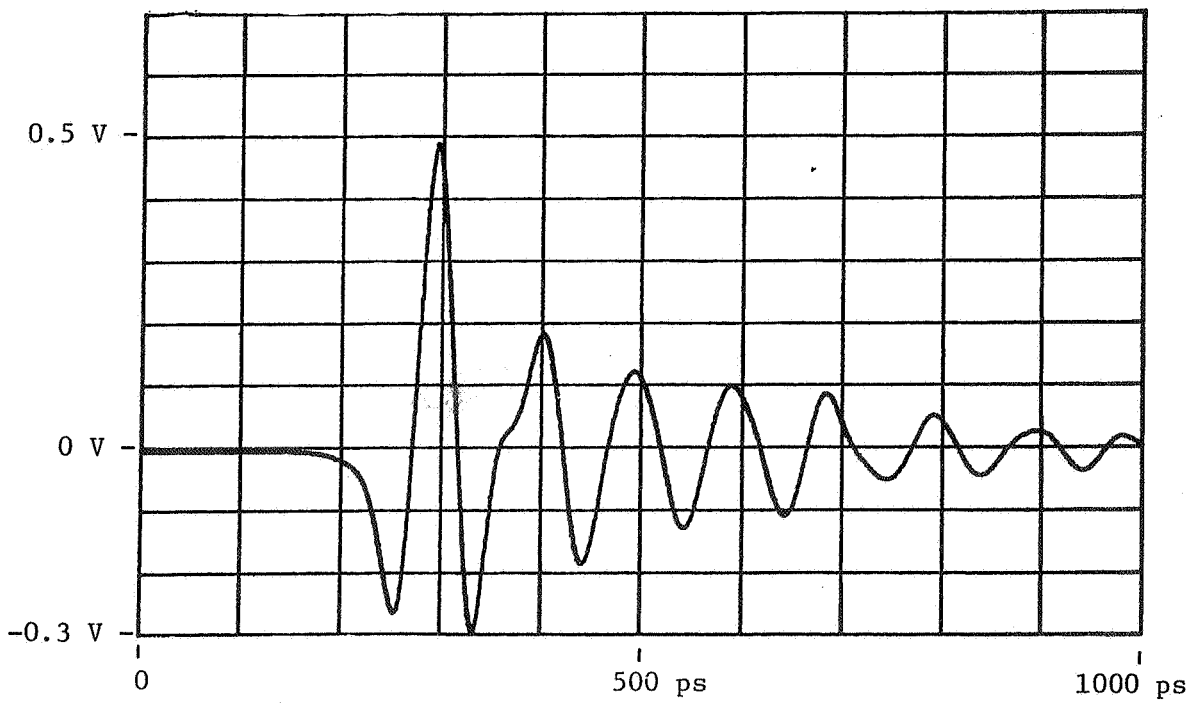
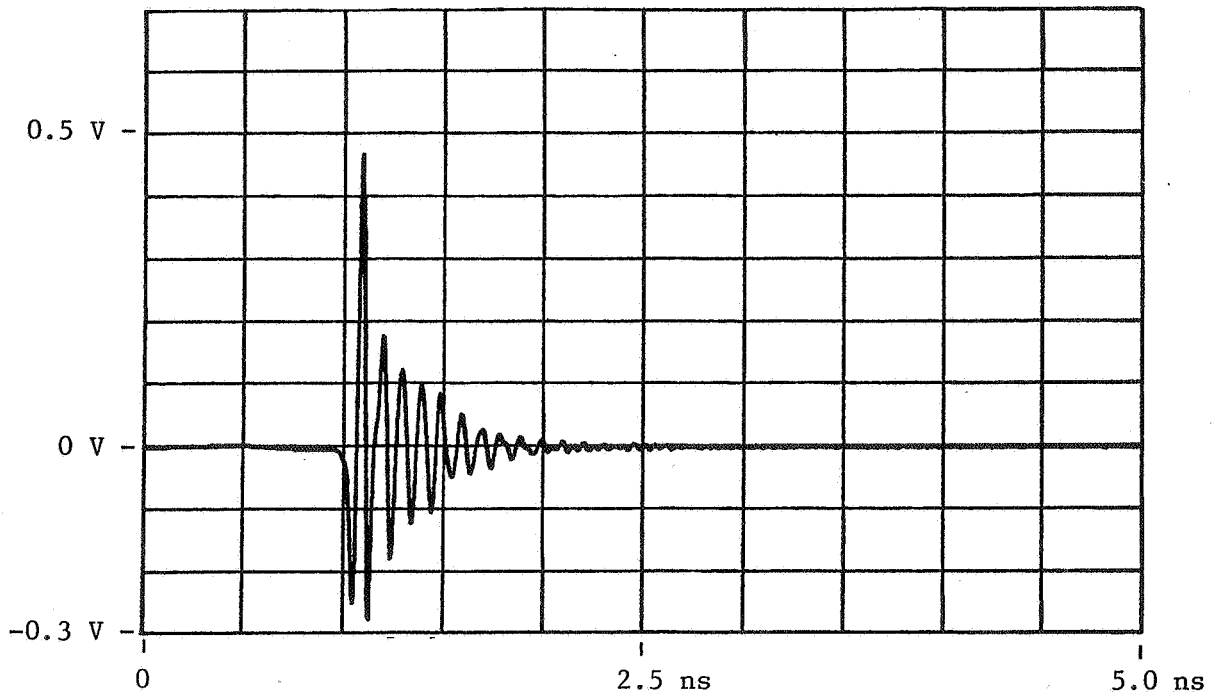


Figure 2.8. SHF impulse generator pulse output waveform.

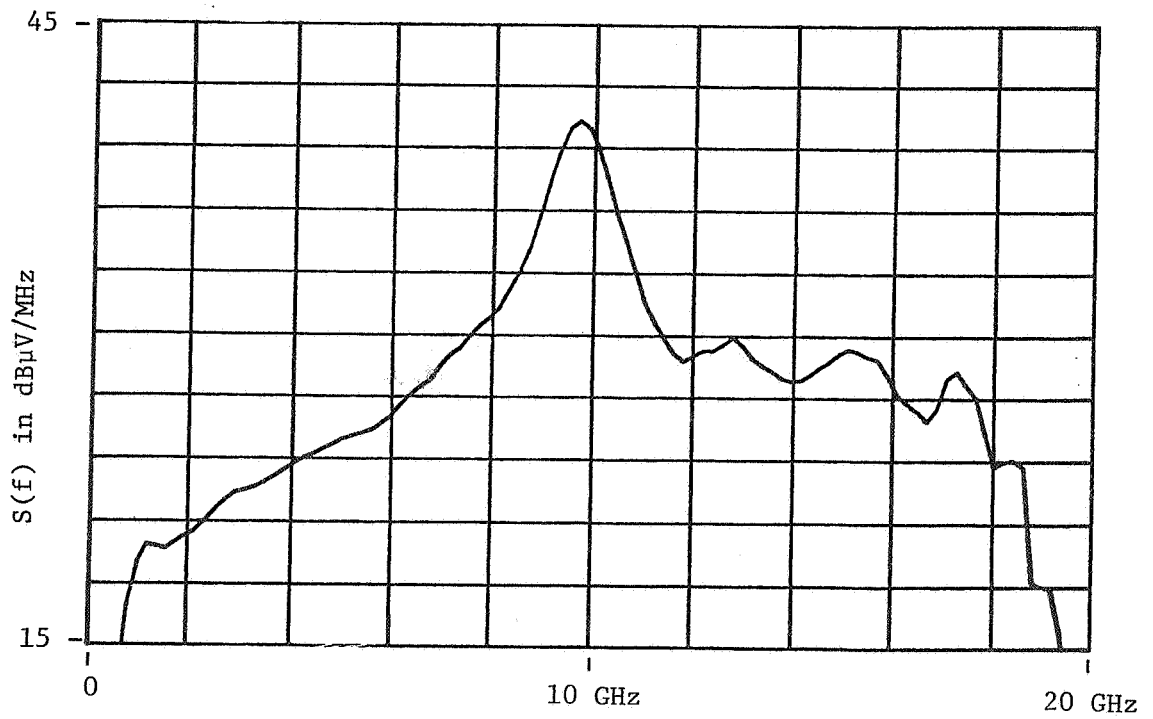
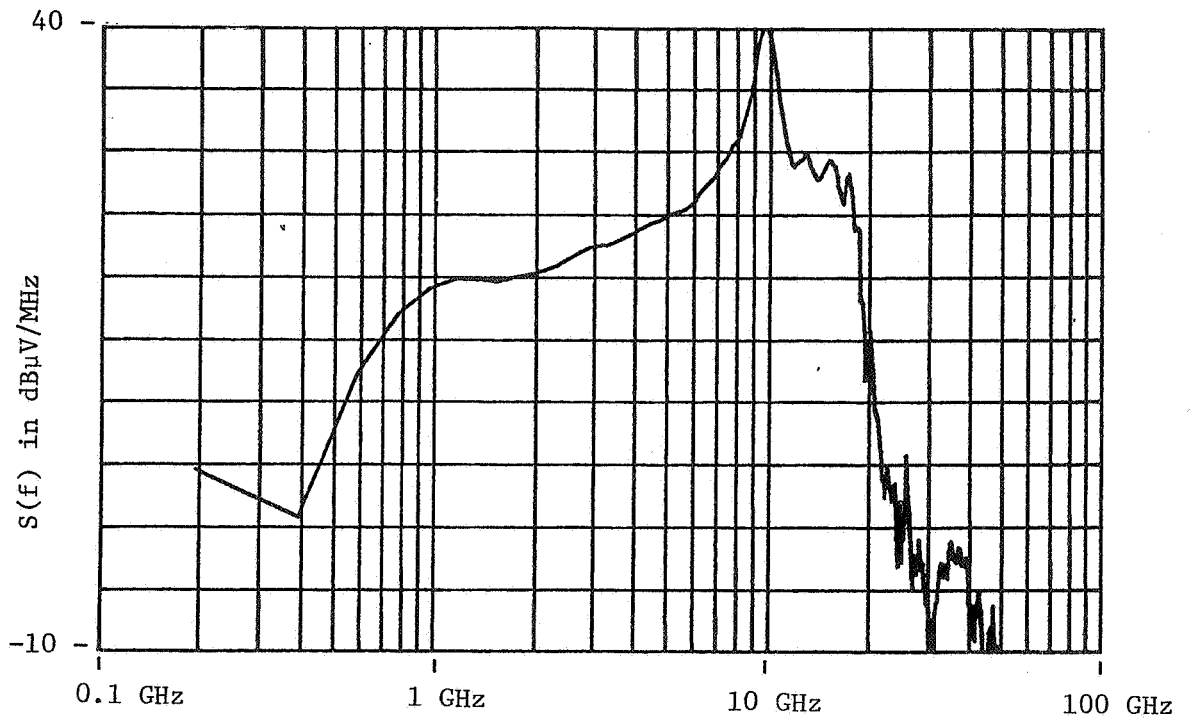
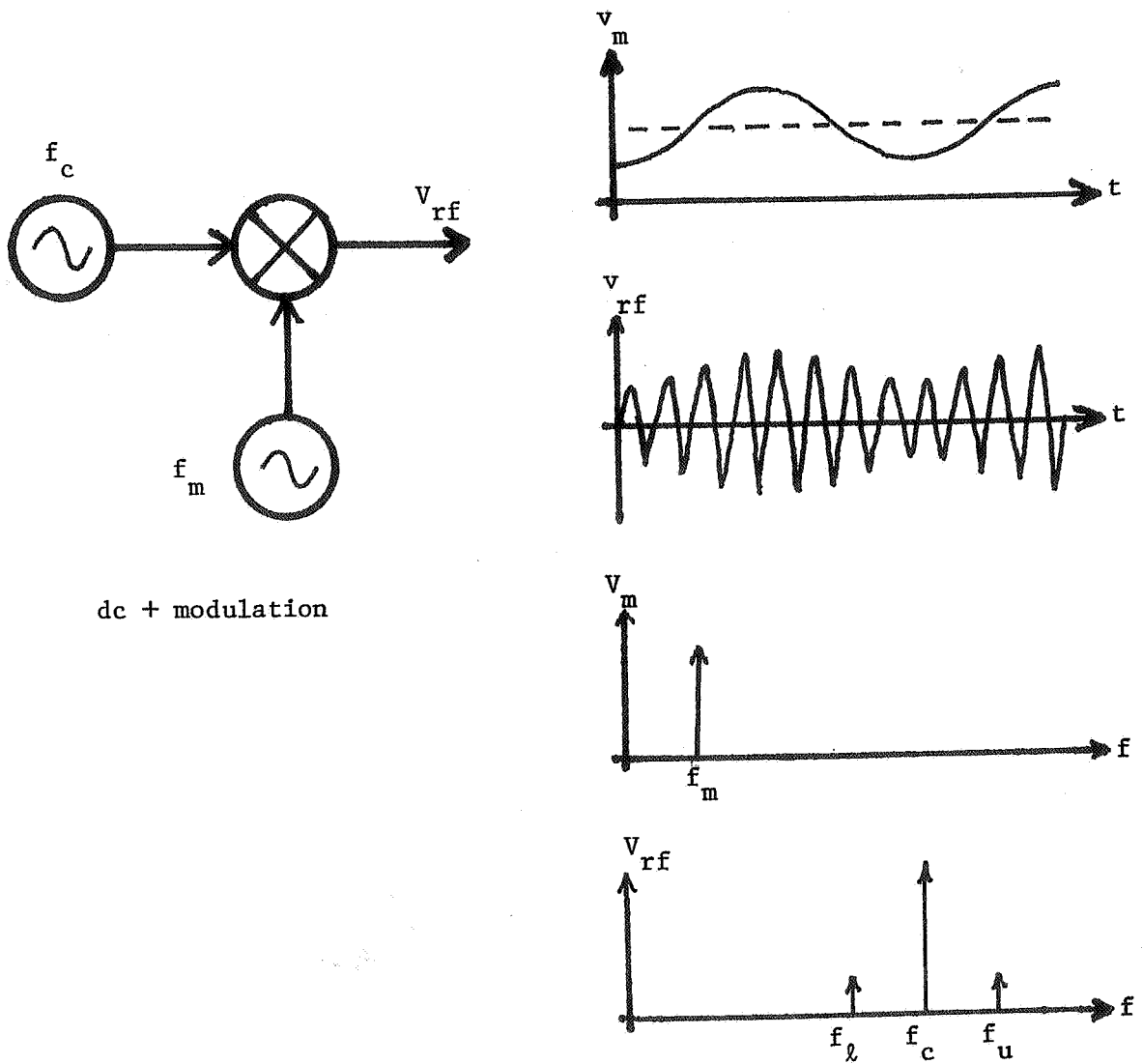


Figure 2.9. SHF impulse generator rf pulse output spectrum.



dc + modulation

Figure 2.10. Amplitude modulation.

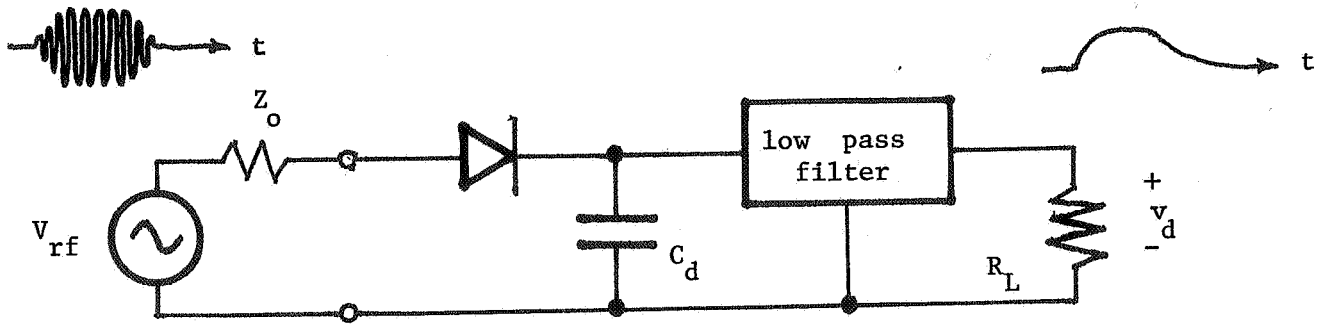


Figure 2.11. Simple diode envelope detector.

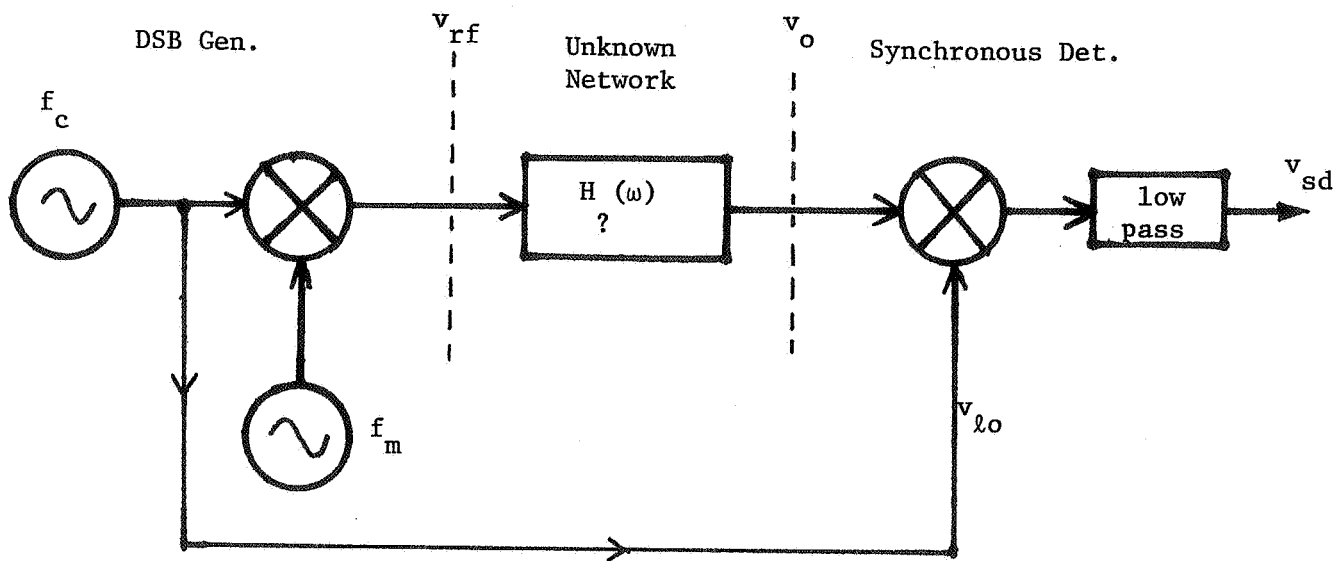


Figure 2.12. Synchronous detector used with DSB generator.

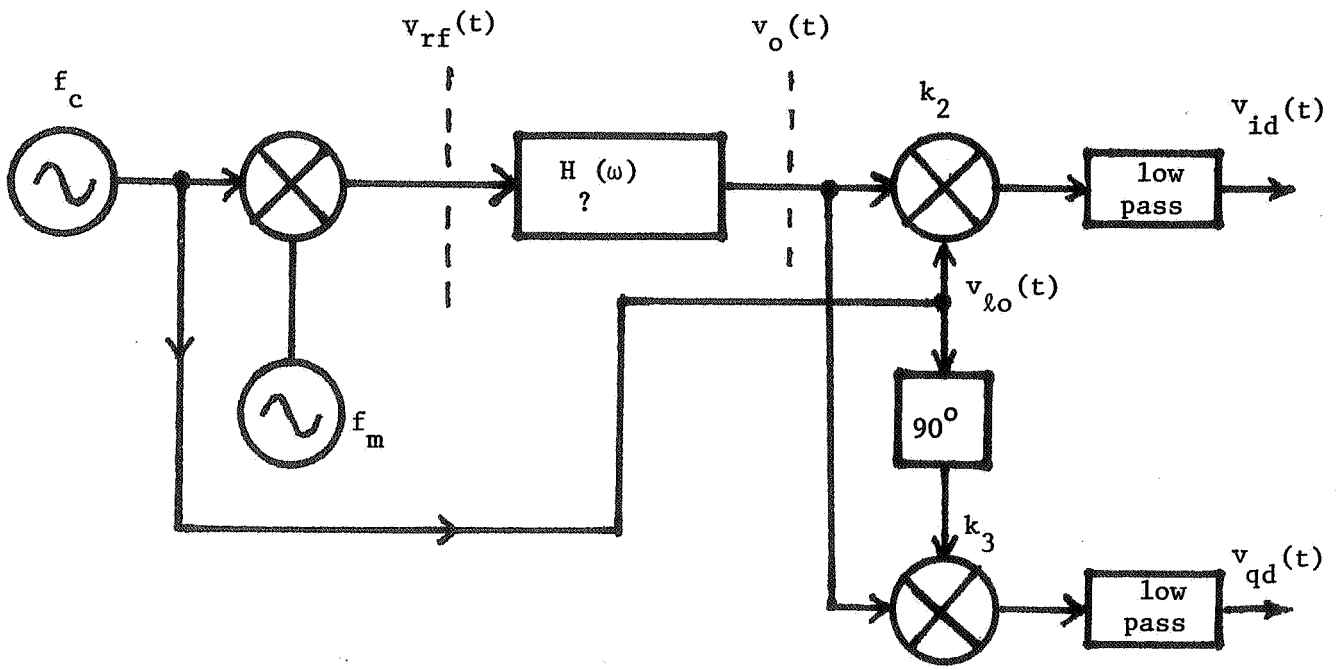


Figure 2.13. I & Q synchronous detector used with DSB generator.

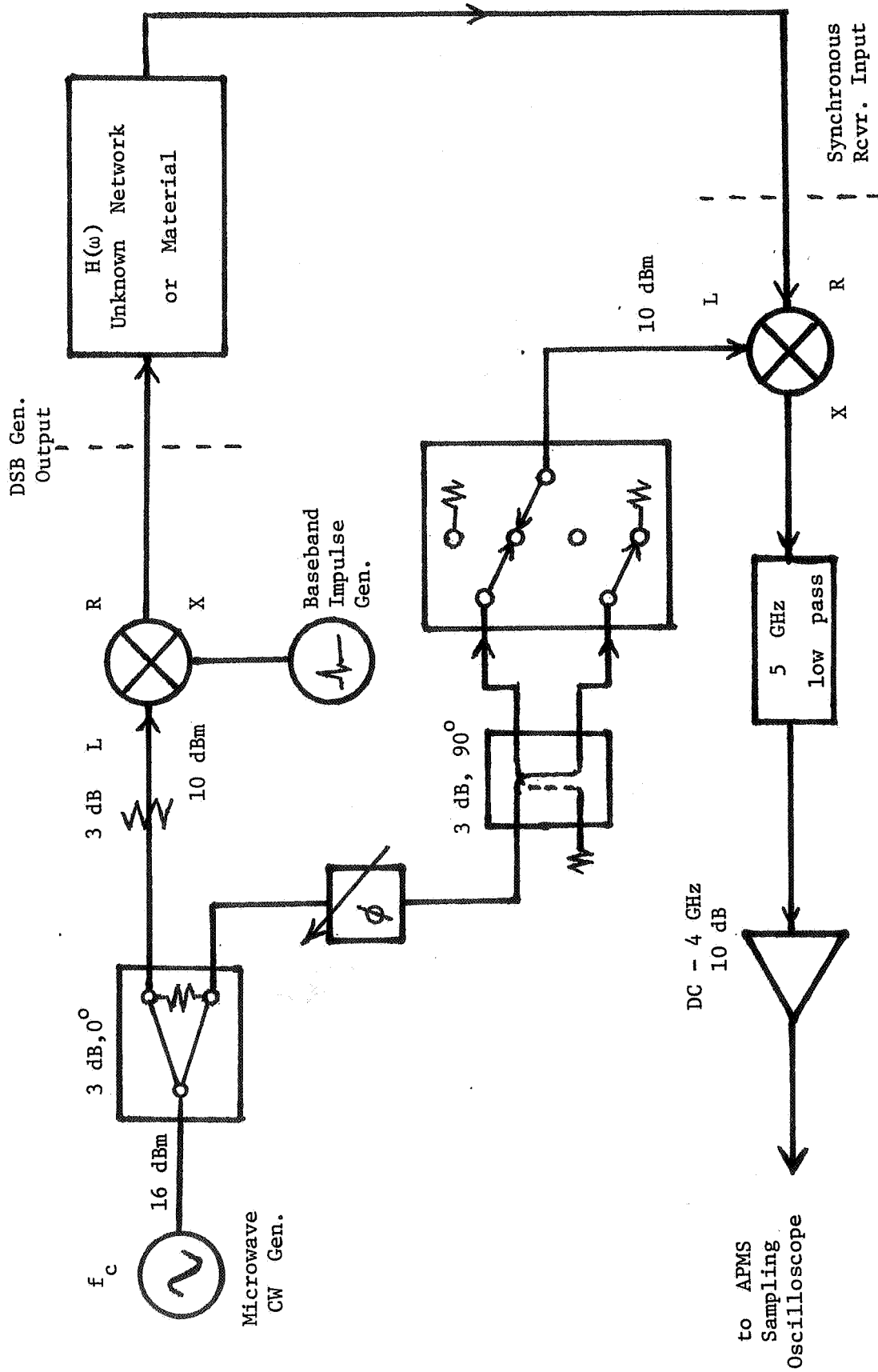


Figure 2.14 Proposed DSB - I & Q Time Domain ANA.

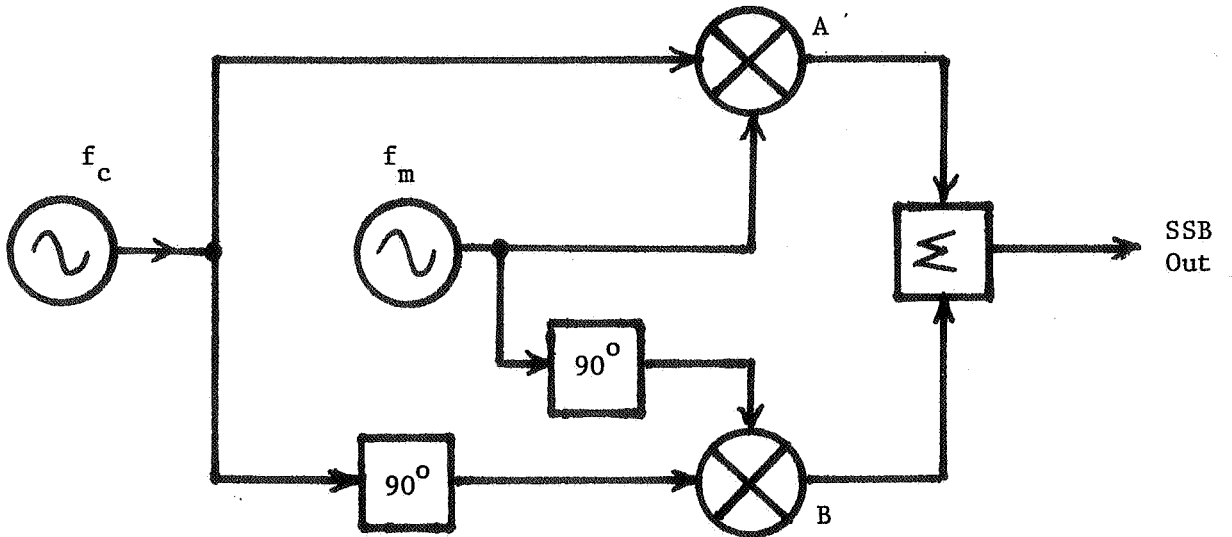


Figure 2.15. Phasing type SSB generator.



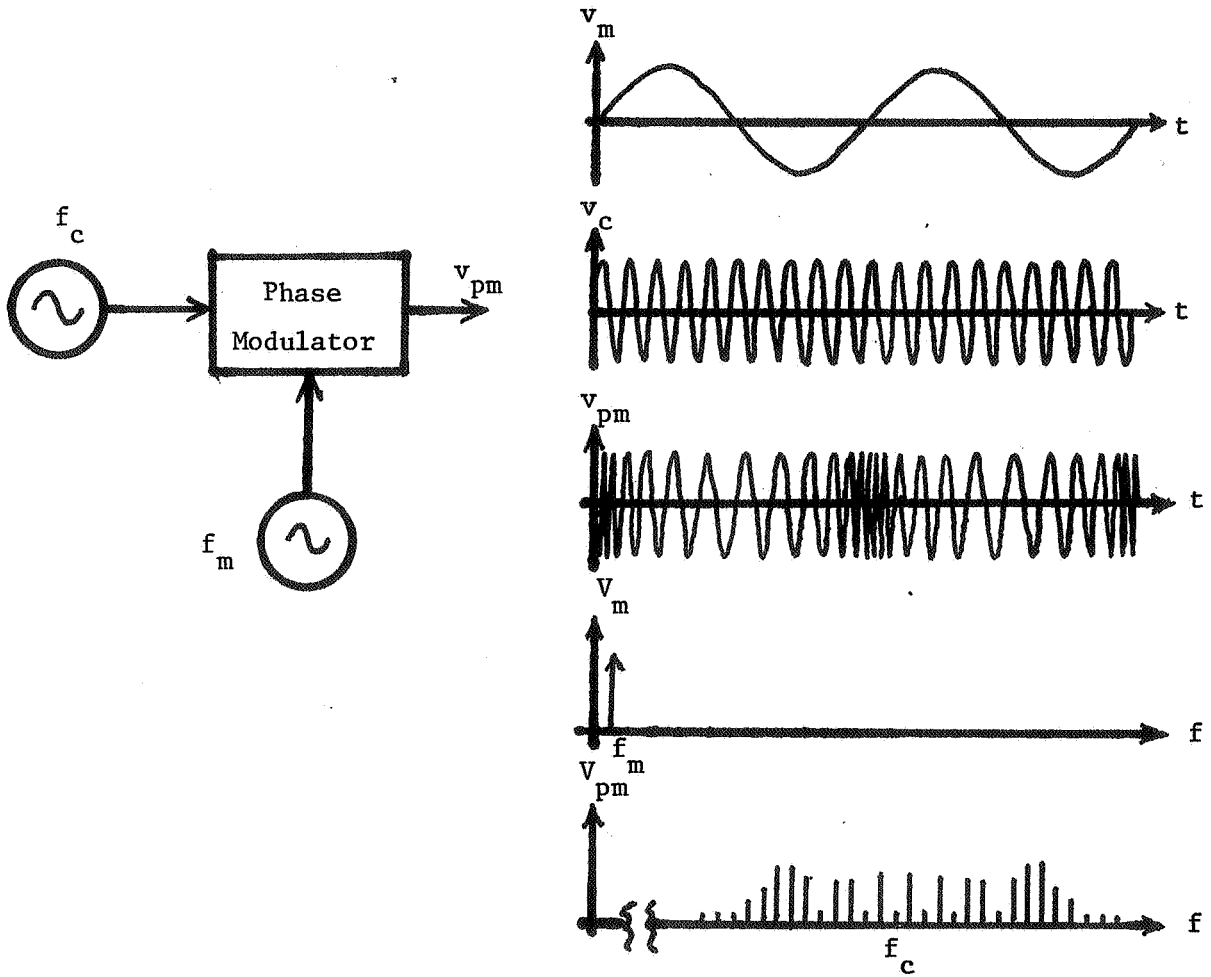


Figure 2.17. Phase modulation.

### 3. IMPROVEMENT OF PICOSECOND-DOMAIN SAMPLING HEADS

N. S. Nahman

#### 3.1 Introduction

For time domain measurements of repetitive low-level millivolt signals with picosecond-domain resolution (tens of gigahertz bandwidth), sampling oscilloscopes are used. The temporal resolution is fundamentally established in the sampling gate structure (i.e., sampling head) and depends upon both the network and the gating properties of the components comprising the sampling head. Also, full utilization of the inherent sampling-head step response or temporal resolution requires low noise (jitter) electronic circuits which control the time positions of the sampling sequence because time base noise introduces a bandwidth limitation to the sampling process [3.1]. Automatic pulse measurement systems can minimize the effects of time base noise and also provide signal processing to enhance the signal-to-noise ratio [3.2,3.3].

However, presently available sampling heads possess several limitations; for example, their dynamic range is limited to signal levels of  $\pm 1$  V. Also, at the instant of sampling, a spurious strobe-kickout signal (of several millivolts in amplitude and several nanoseconds in duration) emanates from the signal input port due to slight sampling bridge (gate) imbalances.

Recently, a new concept has been introduced which has promise to provide improvements in sampling-gate technology [3.4]. The new concept is an optically strobed (switched) photoconductive sampling gate. This type of gate eliminates the problems of the  $\pm 1$  V dynamic range and strobe-kickout.

In  $\mu$ - $\epsilon$  time domain spectroscopy, the excitation or probing signal must possess a spectral amplitude whose strengths are great enough to provide response signal spectral components in the tens of gigahertz range. There are two interconnected ways to visualize the excitation signals. They are interconnected because, in practice, features of both views are necessarily present (fig. 3.1). On the one hand, a suitable probing signal would be an impulse of suitable strength, i.e., one whose integral or area is large enough (fig. 3.1a) [3.5]. Here the signal possesses a very short duration (picoseconds) to insure that the required gigahertz components are present. On the other hand, a suitable probing signal could be a pulse of non-zero duration and a suitable peak value (fig. 3.1b). For example, an impulse of strength  $S$  would provide a constant spectrum amplitude of value  $S$  (fig. 3.1a). If the highest spectral component of interest must have at least a strength of  $S$ , then a rectangular pulse of area  $A\tau > S$  could be used (fig. 3.1b). Because the theoretical impulse function cannot be physically realized, non-zero duration, finite-magnitude pulses are always encountered in practice. Consequently, if the output magnitude of a given pulse generator could be increased by a factor of 10, the spectral amplitude would also increase by the same factor (20 dB).

With regard to the dynamic range of presently available sampling heads, state-of-the-art pulse generators are available which do exceed the  $\pm 1$  V dynamic range. For example, the impulsive generator section of the NBS SHF pulse generator (delivered to the USAF Avionics Laboratory for  $\mu$ - $\epsilon$  TD spectroscopy applications) has a built-in 10 dB attenuator to reduce the magnitude of the impulsive output so that it does not exceed the sampling head dynamic range. Furthermore, the dynamic range of such sampling heads undergoes compression if the display is offset by 1 V to take advantage of the 2 V range provided by the  $\pm 1$  V specification. Typical observed compression characteristics for a 10 GHz sinewave are shown in figure 3.2 [3.6].

#### 3.2 Principles of Operation for Sampling (Oscilloscope) Heads

The sampling gate of a sampling oscilloscope can be represented by the equivalent circuit of figure 3.3. The unknown signal to be measured is represented by  $v_{in}(t)$  where  $t$  represents real time. The sampling gate is the variable resistor represented by the conductance function,  $g(t)$ . A strobe,  $s(t, \tau)$  from the oscilloscope time base controls the sampling gate conductance. The instant of sampling is represented by the variable  $\tau$ . For the time prior to  $\tau$ , the gate is closed, i.e.,  $g = 0$ . At  $t = \tau$ , the strobe opens the gate allowing current,  $i_s(t, \tau)$ , to flow. This current deposits charge on the sampling capacitor,  $C_s$ . When the gate is again closed, a dc voltage,  $V_s$ , remains on  $C_s$  that is proportional to an average of the signal input over the duration of sampling.  $V_s$  is then measured by a high impedance voltmeter and displayed on the cathode ray tube (CRT) screen as a single dot.

A single sample is taken of the input waveform each time the waveform recurs. The time base automatically increments  $\tau$  by a small amount  $\Delta\tau$  after each recurrence so that the waveform is successively sampled at a different point each time it recurs. The original waveform,  $v_{in}(t)$ , is thus converted to an equivalent waveform,  $V_S(\tau)$ , that is, stretched into an equivalent time variable  $\tau$ .

The above discussion can be expressed mathematically. The sampling gate conductance is assumed to be proportional to the strobe signal and always of the same waveshape for each occurrence (fig. 3.4).

$$g(t - \tau) = ks(t - \tau) \quad (3.1)$$

where  $k$  is constant. If the duration,  $t_s$ , of the strobe pulse is much less than the minimum circuit time constant,  $C_S/g_{max}$ , then  $C_S$  can be considered to be a short-circuit during the sampling interval,  $t_s$ . The sampling current,  $i_s$ , is thus given by

$$i_s(t, \tau) = v_{in}(t) g(t, \tau). \quad (3.2)$$

Assuming a perfect gate in the closed condition, then

$$i_s(t, \tau) = 0, \text{ for } t < \tau \text{ and } t > \tau + t_s. \quad (3.3)$$

The sampling capacitor,  $C_S$ , acts as an integrator such that the dc sampled voltage,  $V_S$ , is

$$V_S = \frac{1}{C_S} \int_{-\infty}^{\infty} i_s(t) dt. \quad (3.4)$$

Substituting eq (3.2) into eq (3.4) gives

$$V_S(\tau) = \frac{1}{C_S} \int_{-\infty}^{\infty} v_{in}(t) g(t - \tau) dt. \quad (3.5)$$

For the special case when  $g(t)$  is a true impulse, the  $V_S$  is an exact representation of  $v_{in}$ . A true impulse gating function is the ideal situation and is sought after by sampling gate designers. In actual practice, an impulse gating function can only be approximated. Equation (3.5) is in the form of the correlation integral;  $V_S$  is the cross correlation of  $v_{in}$  and  $g$ . If  $g(t)$  is an even function, then eq (3.5) can also be considered to be the convolution integral. For this analysis, we will consider the more general case of cross correlation.

As an example, consider the case shown in figure 3.4 where  $s(t - \tau)$ , and hence  $g(t - \tau)$ , is an exponential pulse beginning at  $t = \tau$ .

$$g(t - \tau) = G_0 \exp [-(t - \tau)/\sigma] u(t - \tau). \quad (3.6)$$

Here  $u(t - \tau)$  represents the unit step function beginning at  $t = \tau$ . The input signal is assumed to be a rectangular pulse of duration  $t_w$  and starting at  $t_0$ ;

$$v_{in}(t) = V_0 [u(t - t_0) - u(t - t_0 - t_w)]. \quad (3.7)$$

Substituting eqs (3.6) and (3.7) into eq (3.5) and integrating gives the result

$$V_s(\tau) = \bar{V}_s \exp[(\tau - t_0)/\sigma], \text{ for } \tau < t_0 \quad (3.8)$$

$$V_s(\tau) = \bar{V}_s \frac{1 - \exp[(\tau - t_0 - t_w)/\sigma]}{1 - \exp(-t_w/\sigma)}, \text{ for } t_0 < \tau < (t_0 + t_w) \quad (3.9)$$

$$V_s(\tau) = 0, \text{ for } \tau > (t_0 + t_w) \quad (3.10)$$

where

$$\bar{V}_s = \frac{V_0 G_0 \sigma}{C_s} [1 - \exp(-t_w/\sigma)] \quad (3.11)$$

Equations (3.8)-(3.10) are shown as the bottom curve of figure 3.4.

The sampler impulse response is obtained by allowing the pulse duration  $t_w$  to approach zero in which case eq (3.9) goes to zero. The impulse response waveform is thus simply the mirror image of the sampling gate conductance function waveform.

The sampler step response is obtained in a similar manner. In this case,  $t_w$  is allowed to approach infinity:

$$V_s(\tau) = \bar{V}_s(\text{step}) \exp[(\tau - t_0)/\sigma], \text{ for } \tau < t_0 \quad (3.12)$$

$$V_s(\tau) = \bar{V}_s(\text{step}) = V_0 G_0 \sigma / C_s, \text{ for } \tau > t_0 \quad (3.13)$$

The sampling efficiency  $\eta$  of the gate is defined as

$$\eta = \frac{\bar{V}_s(\text{step})}{V_0} = \frac{G_0 \sigma}{C_s} \quad (3.14)$$

### 3.3 Presently Available Devices for Sampling Gates

The actual sampling gate variable conductance  $g(t)$  can be one of several different components [3.2]. At low frequencies in the kilohertz and megahertz region, vacuum tubes, diodes, and transistors or FET's are used. In the gigahertz and subnanosecond region, commercial sampling oscilloscopes use balanced diode bridges in 2, 4, or 6 diode configurations [3.7]. The diodes are normally reverse biased. Upon command of the time base, a balanced set of strobe pulse generators produce narrow voltage impulses large enough to forward bias all of the diodes. This has the effect of a switch momentarily connecting the signal input to the sampling capacitor,  $C_S$ . The dynamic range of the fast diode sampling gates is limited by the low reverse voltage breakdown of the diodes and the forward contact potential. Severe waveform distortion occurs when the input signal is large enough to cause a diode to conduct without being strobed. Electrical strobe kickout is caused by slight imbalances in the strobe generators and the bridge circuit.

### 3.4 Optically Strobed Sampling Gate

An alternate sampling technique is an optically strobed sampling gate. The sampling gate,  $g(t)$ , in figure 3.1 is a photoconductor which is illuminated by an optical strobe impulse,  $s(t, \epsilon)$ . The time resolution achievable with such a sampling device is determined by the duration of the optical impulse and the free-carrier lifetime of the photoconductor. Optical pulse durations of less than one picosecond have been achieved with a mode-locked dye laser [3.8], and free-carrier lifetimes as short as 50 ps or less have been demonstrated with GaAs [3.9].

This type of sampling device has the advantage that the strobe impulse energy is optical and, therefore, the sampled voltage will be free from errors, normally found in the electrically operated sampling gate, which are associated with the feedthrough of the strobe impulse to the sampling capacitor. Likewise, there is no kickout of the strobe. Also, the maximum permissible voltage of the waveform to be measured can be much greater than is the case with conventional sampling oscilloscopes, the dynamic range being limited only by voltage breakdown of the photoconductor. In addition, the linear V-I characteristic of a photoconductor eliminates the distortion errors found in an ordinary sampling gate caused by diode nonlinearities.

### 3.5 Summary

To date, it has been demonstrated [3.4] that it is feasible to use an optically strobed photoconductor to sample fast transition, repetitive, electrical transients. Sampling tests have been made on step-like and impulsive waveforms. These tests indicate that an optically strobed, photoconductive gate is a promising technique for the measurement of fast transition waveforms and is not limited to the measurement of low voltage pulses, as are present sampling gates. Improvements in sensitivity and in transition duration (risetime) can be expected with the application of the high-power picosecond duration optical pulses that are presently available.

### 3.6 References

- [3.1] Gans, W. L., and Andrews, J. R., Time domain automatic network analyzer for measurement of rf and microwave components, NBS Technical Note 672, Nat. Bur. of Stand., Boulder, CO, 113-114 (Sept. 1975).
- [3.2] Andrews, J. R., Automatic network measurements in the time domain, Proc. IEEE 66, No. 4, 414-423 (April 1978).
- [3.3] Nahman, N. S., Picosecond-domain waveform measurements, Proc. IEEE 66, No. 4, 441-454 (April 1978).
- [3.4] Lawton, R. A., and Andrews, J. R., Optically strobed sampling oscilloscope, IEEE Trans. on Instr. and Meas. 25, No. 1, 56-60 (March 1976).
- [3.5] McGillem, C. D., and Cooper, G. R., Continuous and Discrete Signal and System Analysis (Holt, Rinehart, and Winston, Inc., New York, 1974).
- [3.6] Nahman, N. S., and Jickling, R. M., Frequency domain measurement of baseband instrumentation, NBSIR 73-330, NBS Boulder, CO (July 1973).

- [3.7] Mulvey, J., Sampling oscilloscope circuits (Beaverton, Oregon: Tektronix,1970).
- [3.8] Shank, C. V., and Ippen, E. P., Subpicosecond kilowatt pulses from a mode-locked cw dye laser, Appl. Phys. Lett. 24, No. 8, 373-375 (April 15, 1975).
- [3.9] Lawton, R. A., and Scavannec, A. S., A photoconductive detector of fast transition waveforms, Electron. Lett. 11, No. 4, 74-75 (Feb. 20, 1975).

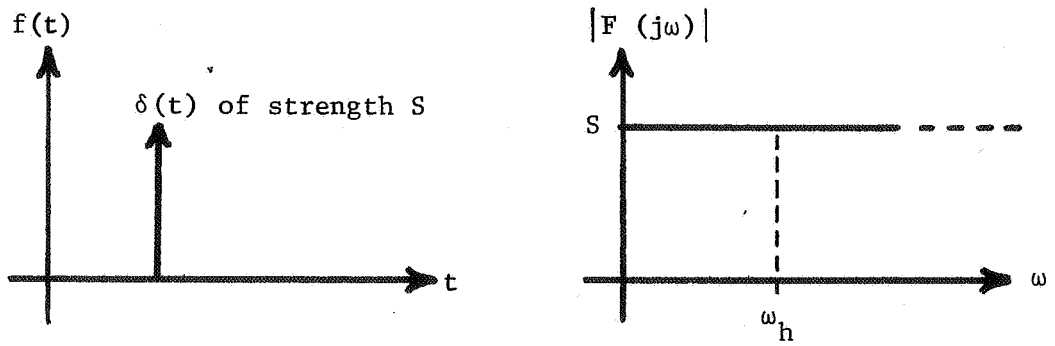


Figure 3.1a. An impulse,  $\delta(t)$ .

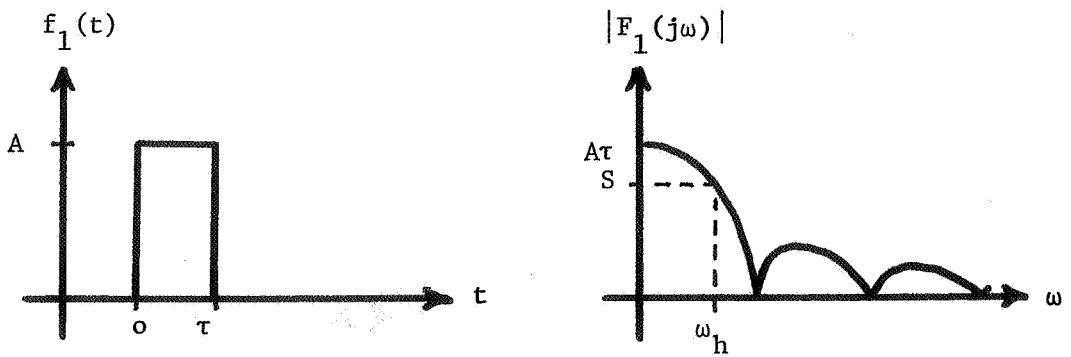


Figure 3.1b. A rectangular pulse.

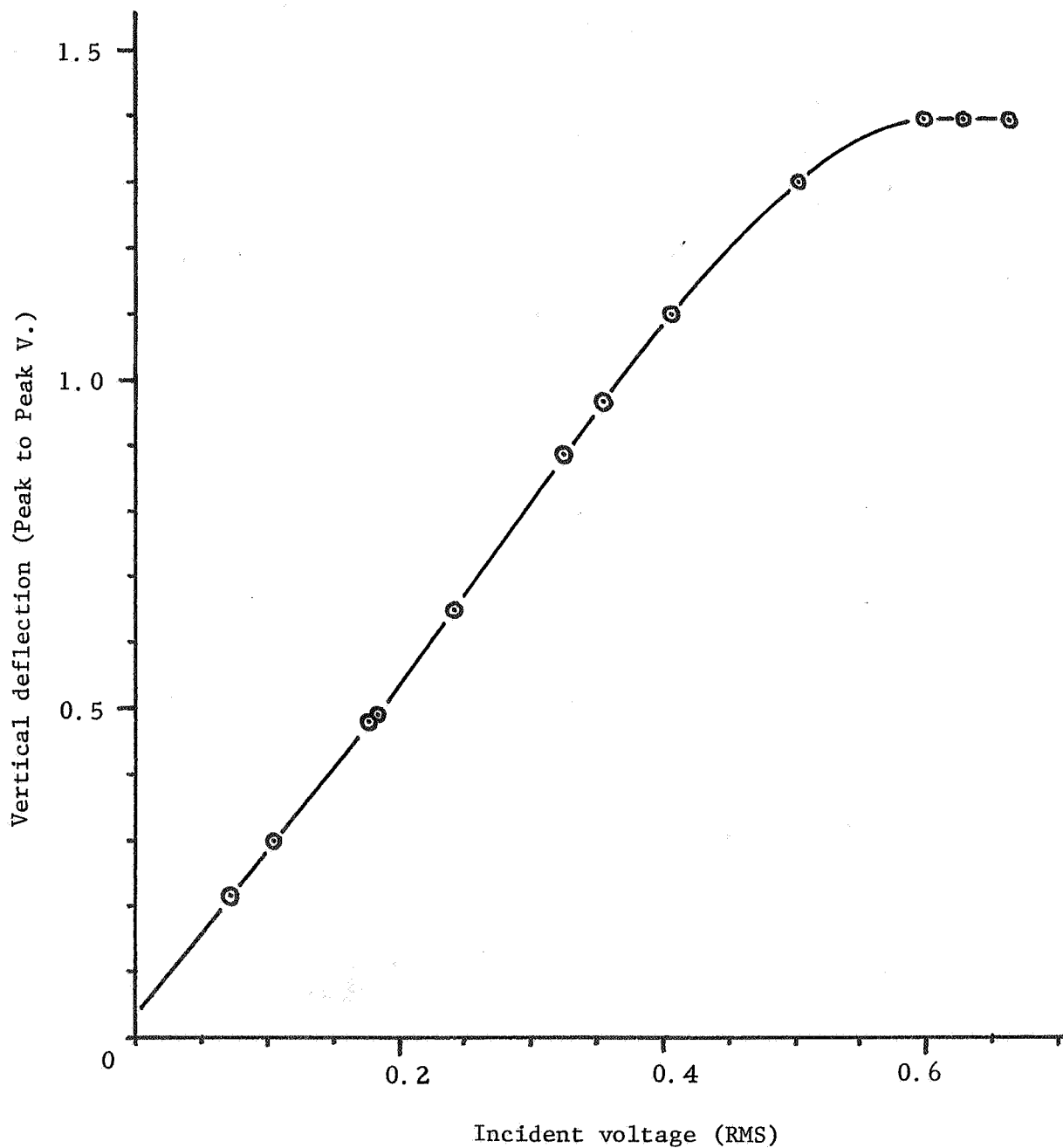


Figure 3.2. Typical results for an oscilloscope deflection response measurement at 10 GHz.

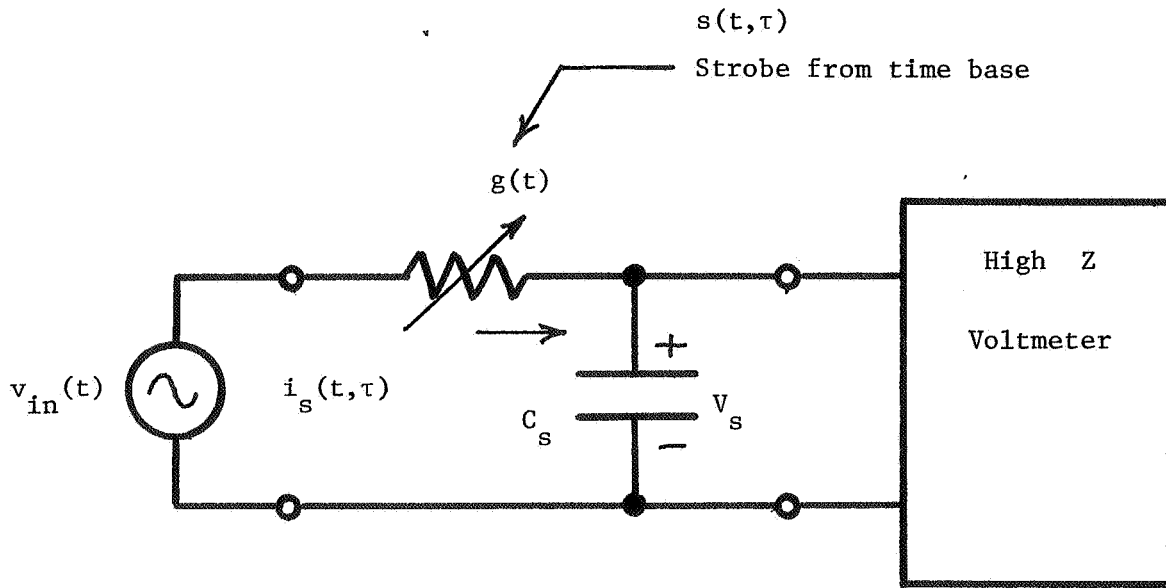


Figure 3.3. Sampling gate equivalent circuit.

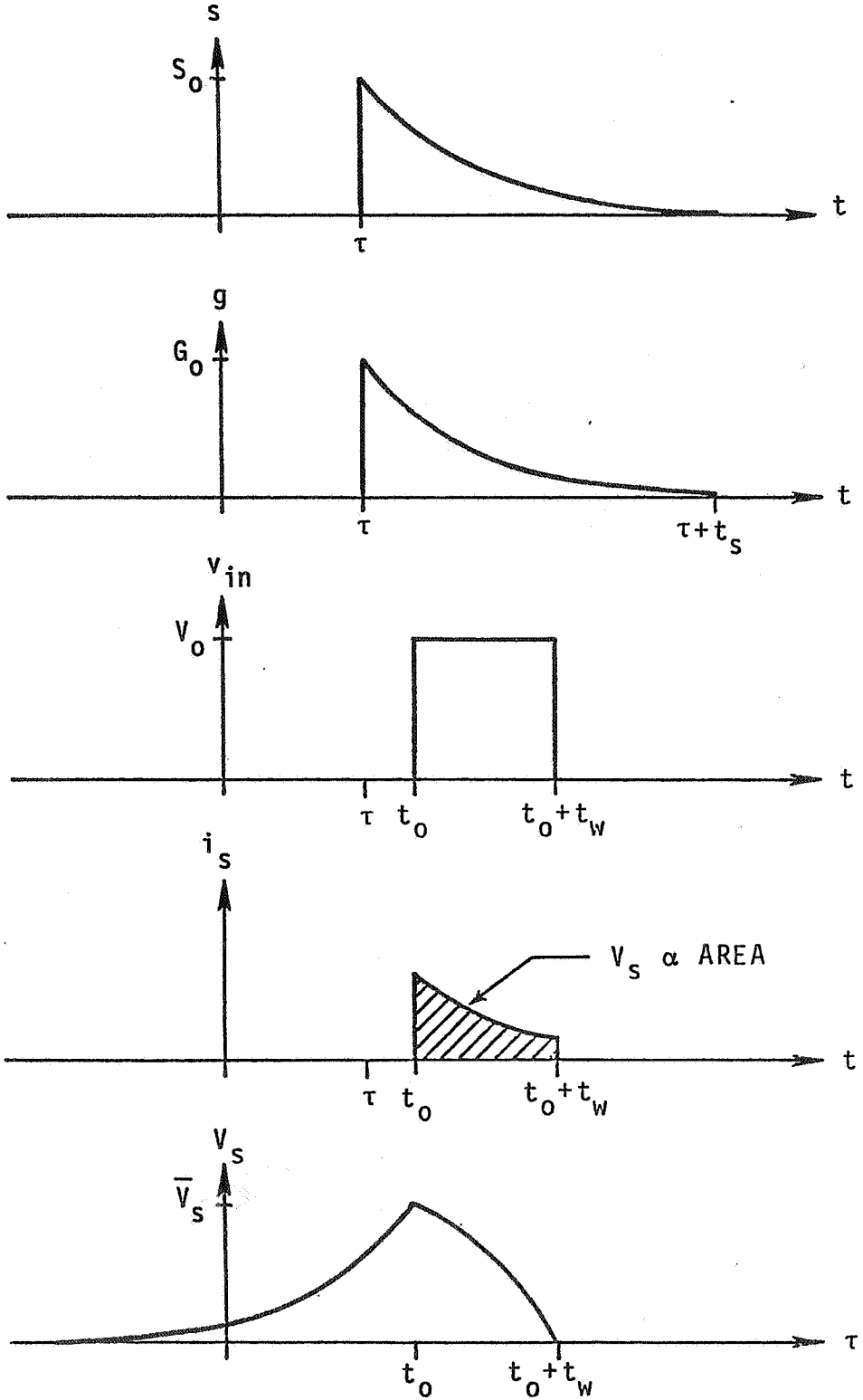


Figure 3.4. Sampling gate pulse response waveforms.

## 4. CORRELATION MEASUREMENT SYSTEMS USING NOISE SIGNAL SOURCES

R. A. Lawton and N. S. Nahman

### 4.1 Introduction

The time domain automatic network analyzer discussed in Chapter 2 employs a computer-controlled sampling oscilloscope to acquire the signal pulse waveforms which are, for the most part, deterministic (not stochastic) signals. The sampling process (equivalent time sampling) is mathematically described by the time integral of the product between the sampling pulse (train) and the signal [4.1]. In this chapter, a correlation measurement system will be discussed with the excitation and response signals being stochastic signals. The excitation source is a noise generator; consequently, it has a randomly varying waveform which can be characterized in terms of statistical measures and correlation properties.

### 4.2 Correlation Functions

Sampling and correlation measurements have the same mathematical description, but they are basically implemented by entirely different methods [4.2]. The sampling method uses a switching or gating network,<sup>1</sup> while correlation in the picosecond region of the time domain employs a nonswitched mixing process in a nonlinear element to provide the multiplication process. Both techniques are described by the following integral equation.

$$\phi_{12}(\tau) = \int_{-\infty}^{\infty} f_1(t)f_2(t + \tau)dt \quad (4.1)$$

where  $\tau$  may be varied continuously or discretely and in which  $\tau$  is the time difference between  $f_1(t)$  and  $f_2(t)$ .<sup>2</sup> Equation (4.1) is commonly called a cross-correlation function of the two functions  $f_1(t)$  and  $f_2(t)$  [4.3]. In sampling, the sampling pulse or gating function is cross-correlated with the signal waveform, i.e., the sampling function is given by

$$s(\tau) = \int_{-\infty}^{\infty} f(t)g(t - \tau)dt \quad (4.2)$$

where  $\tau$  is the time delay of the gating function with respect to the signal  $f_1(t)$ . Here  $\tau$  is positive and represents the sampling point referenced to the beginning of the signal  $f(t)$ .

The cross-correlation function  $\phi_{21}(\tau)$  is defined by

$$\phi_{21}(\tau) = \int_{-\infty}^{\infty} f_1(t + \tau)f_2(t)dt. \quad (4.3)$$

<sup>1</sup>Refer to Chapter 3, section 3.2, for a review of the sampling method.

<sup>2</sup>When both  $f_1(t)$  and  $f_2(t)$  are not square-integrable signals, the form of eq (4.1) is incorrect. Step functions, random noise, and periodic signals are not square-integrable [4.3]. Under such conditions, eq (4.1) is modified to the form

$$\phi_{12}(\tau) = \lim_{T \rightarrow \infty} \frac{1}{2T} \int_{-T}^T f_1(t)f_2(t + \tau)dt .$$

Clearly,

$$\phi_{12}(\tau) = \phi_{21}(-\tau). \quad (4.4)$$

Furthermore, the Fourier transform of the cross-correlation function eq (4.1) is given by

$$\Phi_{12}(j\omega) = \int_{-\infty}^{\infty} \phi_{12}(\tau) e^{-j\omega\tau} d\tau \quad (4.5)$$

$$= F_1^*(j\omega)F_2(j\omega) = F_1(-j\omega)F_2(j\omega) \quad (4.6)$$

where  $F_1(j\omega)$  and  $F_2(j\omega)$  denote the Fourier transforms of  $f_1(t)$  and  $f_2(t)$ , respectively.<sup>3</sup> Similarly,

$$\Phi_{21}(j\omega) = F_1(j\omega)F_2(-j\omega); \quad (4.7)$$

consequently,

$$\Phi_{12}(j\omega) = \Phi_{21}^*(j\omega). \quad (4.8)$$

$\Phi_{12}(j\omega)$  and  $\Phi_{21}(j\omega)$  are complex; each is referred to as a cross-correlation spectral-density function. When  $f_1(t)$  and  $f_2(t)$  are identical, eq (4.1) yields the autocorrelation function of  $f_1(t)$

$$\phi_{11}(\tau) = \int_{-\infty}^{\infty} f_1(t)f_1(t + \tau)dt. \quad (4.9)$$

The Fourier transform of the autocorrelation function eq (4.9) yields  $|F_1(j\omega)|^2$  which is a real and positive function of  $\omega$ .  $|F_1(j\omega)|^2$  is commonly called the energy-spectral-density function; it is related to the spectrum amplitude  $A(\omega)$  through the relation [4.4]

$$A(\omega) = 2 |F_1(j\omega)|. \quad (4.10)$$

---

<sup>3</sup>If  $\phi_{12}(\tau)$  is periodic, the integral form must be modified as discussed in footnote 2.

#### 4.3 Using Noise and Correlation Methods for $\mu$ - $\epsilon$ Measurements

An alternate technique for determining network characteristics and thus  $\mu$  and  $\epsilon$  over a wide band of frequencies is the noise cross-correlation approach. The basic idea of this approach can be introduced with the autocorrelator outlined in figure 4.1 which could be implemented in any desired waveguide, e.g., coaxial line, WR12 (60-90 GHz), etc. As shown by the diagram, a noise signal with a time domain waveform,  $f(t)$ , is split into two channels, one of the channels being delayed with respect to the other. The two signals are then recombined, and the result multiplied and integrated which results in the function  $A + 2\phi_{11}(\tau)$  at the output of the integrator,

$$A + 2\phi_{11}(\tau) = \lim_{T \rightarrow \infty} \frac{1}{2T} \int_{-T}^T f_1(t) f_1(t + \tau) dt. \quad (4.11)$$

The square law device produces the output

$$g(t) = f_1^2(t - \tau_1) + f_1^2(t - \tau) + 2 f(t - \tau_1) f_1(t - \tau) \quad (4.12)$$

which the integrator transforms to

$$\int g(t) dt = \langle f_1^2(t) \rangle + \langle f_1^2(t) \rangle + 2 \int f_1(t) f_1(t + \tau) dt. \quad (4.13)$$

The first two terms are identical and are each equal to the time average value of  $f_1^2(t)$ ; the third term is twice the autocorrelation function,  $\phi_{11}(\tau)$ , of  $f_1(t)$ . Consequently, the output of the integrator is  $2\phi_{11}(\tau)$  plus a constant,  $A$ . The signal path delays,  $\tau_1$  and  $\tau$ , are such that the two signals can be in effect delayed or advanced with respect to each other.

An example of an experimentally measured autocorrelation function for a picosecond domain pulse signal is shown in figure 4.2 [4.3]. Because the autocorrelation function is always an even function of the time delay, only the portion for  $\tau \geq 0$  is shown.

Let us now consider figure 4.3 which is exactly the same as in figure 4.1 except that a network whose impulse response,  $h(\tau)$ , is to be determined has been inserted in the upper channel. Now at the output of the integrator, apart from a constant,  $A_2$ , one has the cross correlation,  $2\phi_{21}(\tau)$ , between  $f_1(t)$  and the output of the unknown network.

$$\phi_{21}(\tau) = \lim_{T \rightarrow \infty} \frac{1}{2T} \int_{-T}^T f_2(t) f_1(t + \tau) dt. \quad (4.14)$$

Here the subscripts 1 and 2 denote the input and output functions of the unknown network. Note that  $f_2(t)$  is the convolution between  $f_1(t)$  and  $h(t)$  denoted by  $f_1(t) * h(t)$ , i.e.,

$$f_2(t) = f_1(t) * h(t) = \int_0^t f_1(t - \lambda) h(\lambda) d\lambda. \quad (4.15)$$

The autocorrelation function will now be denoted as  $\phi_{11}(\tau)$ .

In reference [4.4] it is seen that the Fourier transform of  $\phi_{11}(\tau)$  yields the input power density spectrum,  $S_{11}(\omega)$ , of the signal,  $f(t)$ ; and the Fourier transform of  $\phi_{21}(\tau)$  yields the cross spectrum,  $S_{21}(\omega)$ . The significance of the cross spectrum is that when divided by the

input power density spectrum,  $S_{11}(\omega)$ , it yields the complete system transfer function,  $H(\omega)$ , of the inserted network. In other words,

$$S_{21}(\omega)/S_{11}(\omega) = H(\omega). \quad (4.16)$$

Now let us consider a system in which the signal source is a white noise generator whose power density spectrum has the value  $K$  (independent of frequency). In this case

$$S_{21}(\omega) = KH(\omega) \quad (4.17)$$

which has the inverse transform

$$\phi_{21}(\tau) = 2\pi K h(\tau). \quad (4.18)$$

In other words, for a white noise source, the system impulse response is directly proportional to the cross-correlation function between the input and output signals. From this impulse response or, equivalently, from the system transfer function, all the network parameters of the inserted network such as dielectric constant and permeability could be determined.

While the above description has been given in general for any waveguide, it can be applied to any specific waveguide band. However, every band will be somewhat band limited, and the noise source, for that reason alone, will not be a completely white noise source. Equation (4.16) can then be used to remove the effect of the band-limited source. Some examples of white noise, cross-correlation functions or network impulse responses that one might encounter are those of the low pass R-C integrator and the Debye dielectric lossy transmission line [4.5] which are given in figure 4.4 along with their respective equivalent circuits.

#### 4.3.1 Time Resolution Requirements

The next question one might ask is what time delay temporal resolution is required. To get a rough estimate, suppose that the filtering characteristic of the inserted network is approximately Gaussian in character; then the transfer function  $H(j\omega)$  would be approximated by

$$H(j\omega) = e^{-\omega^2/4k^2}, \quad (4.19)$$

while the corresponding approximate network impulse response would be the inverse Fourier transform of  $H(j\omega)$  which is

$$h(\tau) = \frac{k}{2\pi} e^{-k^2\tau^2} \quad (4.20)$$

The two functions  $H(j\omega)$  and  $h(\tau)$  are each Gaussian functions and possess the  $1/e$  intervals of

$$\Delta\omega = 4k \quad (4.21)$$

and

$$\Delta\tau = 2/k, \quad (4.22)$$

respectively (fig. 4.5). Therefore, for a network bandwidth of

$$\Delta f = \frac{\Delta\omega}{2\pi} = 30 \text{ GHz},$$

which would totally occupy the available bandwidth in the WR-12 waveguide band (60-90 GHz), the corresponding impulse response duration would be

$$\Delta\tau = \frac{2}{15\pi \times 10^9} = 21.2 \text{ ps.}$$

This, in turn, would require that the delay measurement resolution be of the order of two picoseconds or better, which corresponds to a distance measurement of 0.6 mm for electromagnetic wave propagation in air.

#### 4.3.2 Other Realization Considerations

Square law detector: Diodes, thermistors, and resistive bolometers with pyroelectric sensors may be used to provide the multiplying function. The use of resistive heaters and pyroelectric sensors is outlined in detail in [4.3]. The same reference describes how the device capacitance can be used for the required integration. The use of diodes can provide greater sensitivity than the use of bolometers or pyroelectric detectors, but the latter two devices provide better square law response with the pyroelectric detector being the more sensitive of the two.

Noise source: The solid state noise source developed by Kanda [4.6] is a strong source and thus provides large noise temperatures, typically 290,000 K.

#### 4.4 References

- [4.1] Nahman, N. S., Picosecond-domain waveform measurements, Proc. IEEE 66, No. 4, 441-454 (April 1978).
- [4.2] Ibid, p. 444.
- [4.3] Lawton, R. A., Autocorrelation and power measurement with pyroelectric and dielectric bolometers, IEEE Trans. on Instr. and Meas. IM-22, No. 4, 299-306 (Dec. 1973).
- [4.4] Lee, Y. W., Statistical Theory of Communication (John Wiley and Sons, Inc., New York, 1967).
- [4.5] McCaa, W. D., Jr., and Nahman, N. S., Generation of reference waveforms by uniform lossy transmission lines, IEEE Trans. on Instr. and Meas. IM-19, No. 4, 382-390 (Nov. 1970).
- [4.6] Kanda, M., An improved solid-state noise source, IEEE Trans. Microwave Theory and Tech. MTT-24, No. 12, 990-995 (Dec. 1976).

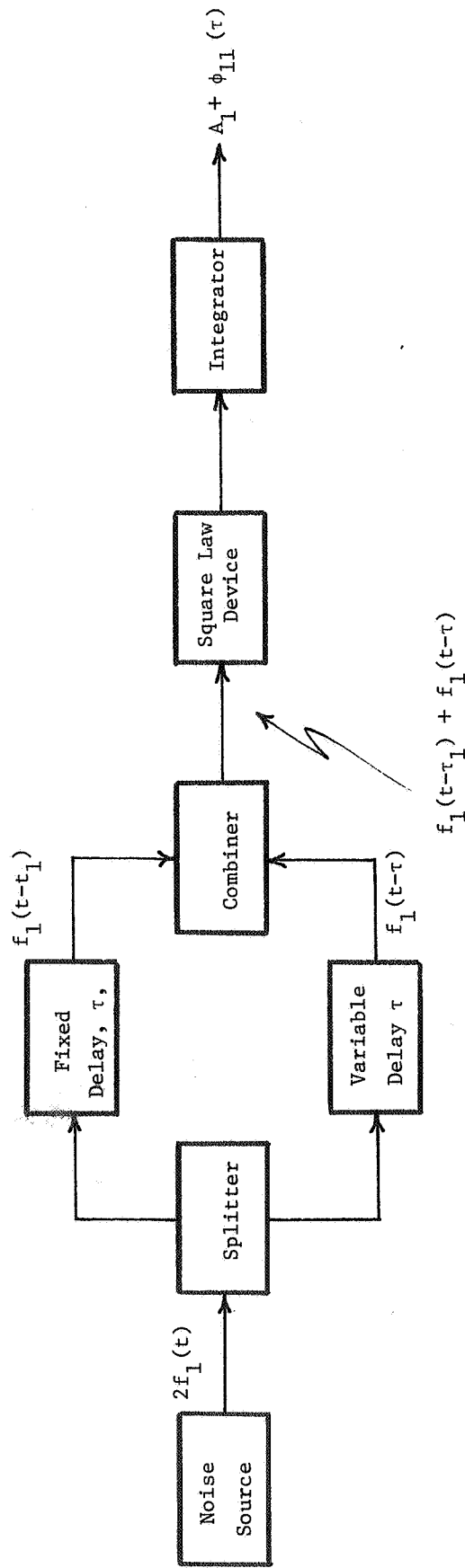


Figure 4.1. Autocorrelation system.

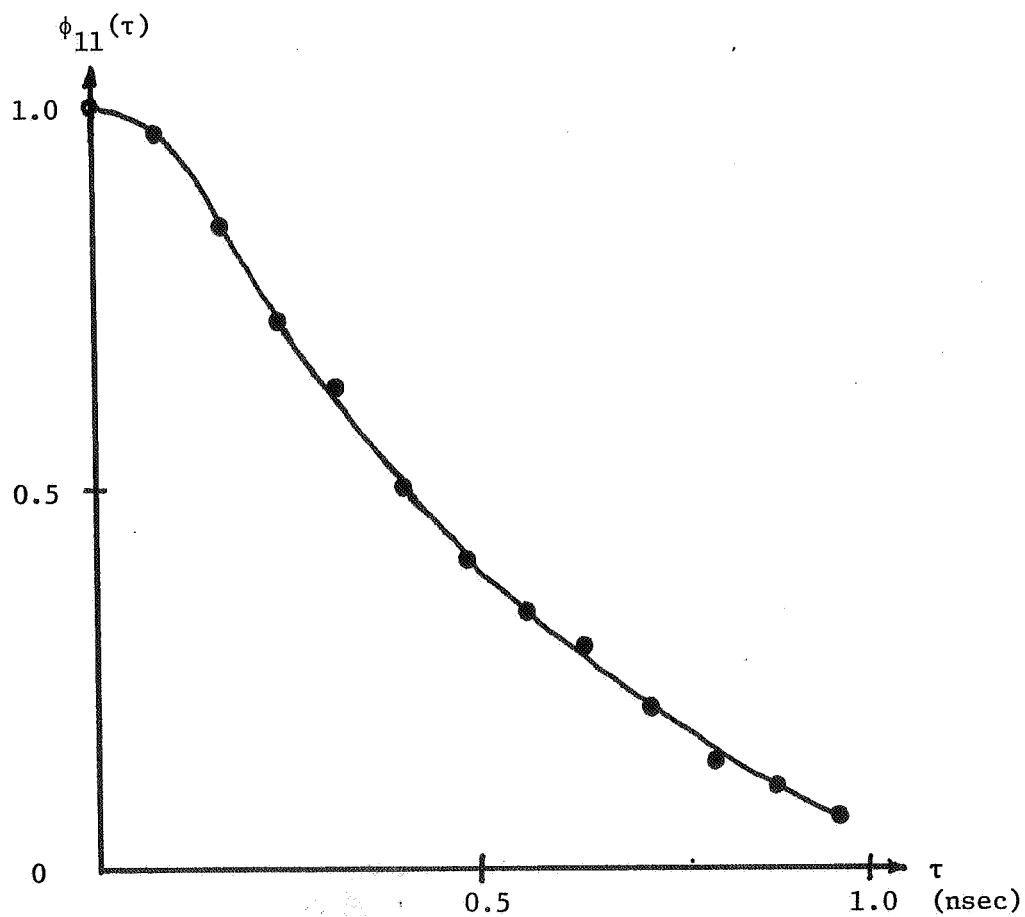


Figure 4.2. Autocorrelation function as measured.

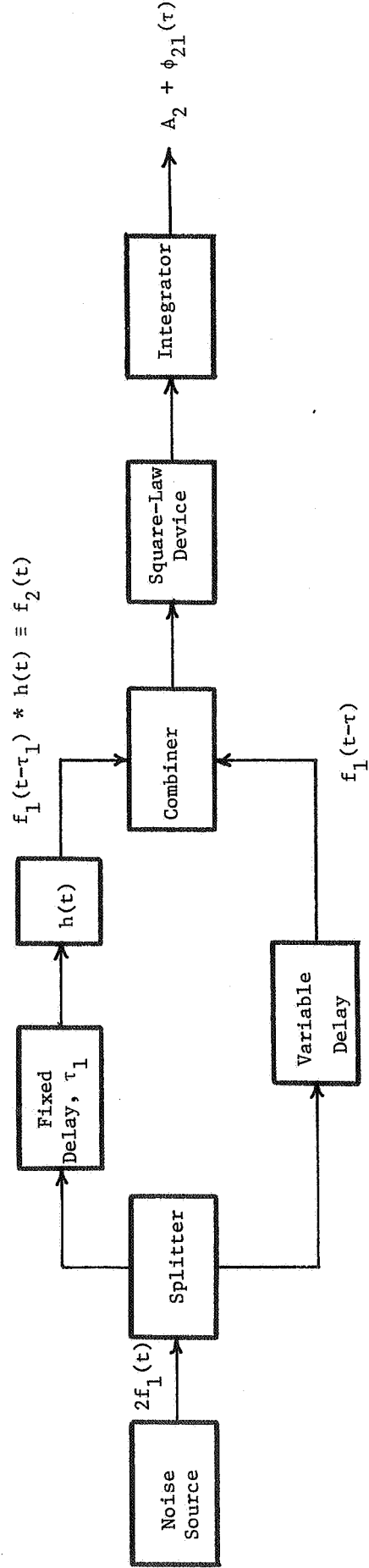
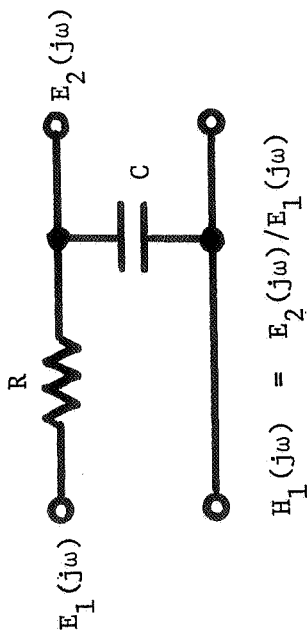


Figure 4.3. Cross-correlation system.



$$H_1(j\omega) = E_2(j\omega)/E_1(j\omega)$$

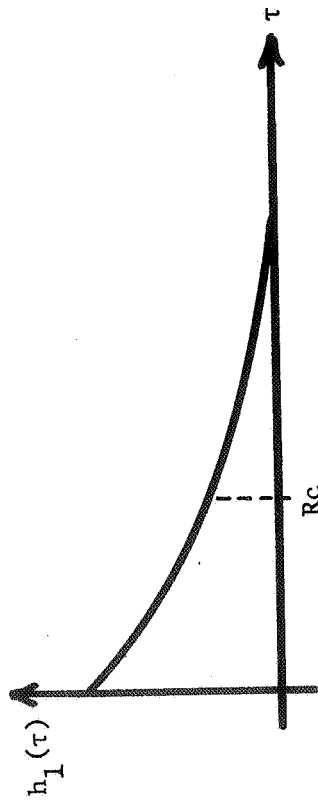
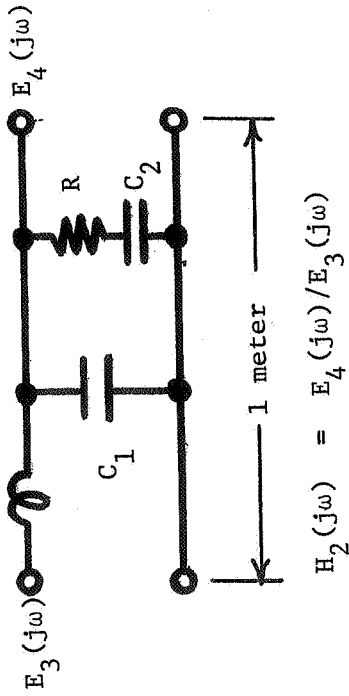


Figure 4.4a. Impulse response of low-pass RC network.



$$H_2(j\omega) = E_4(j\omega)/E_3(j\omega)$$

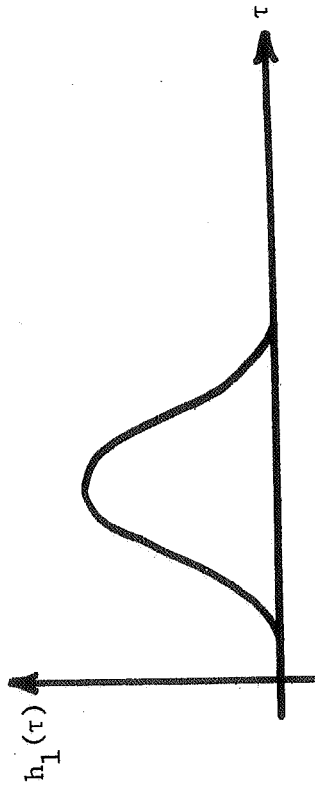


Figure 4.4b. Impulse response of a Debye dielectric lossy transmission line.

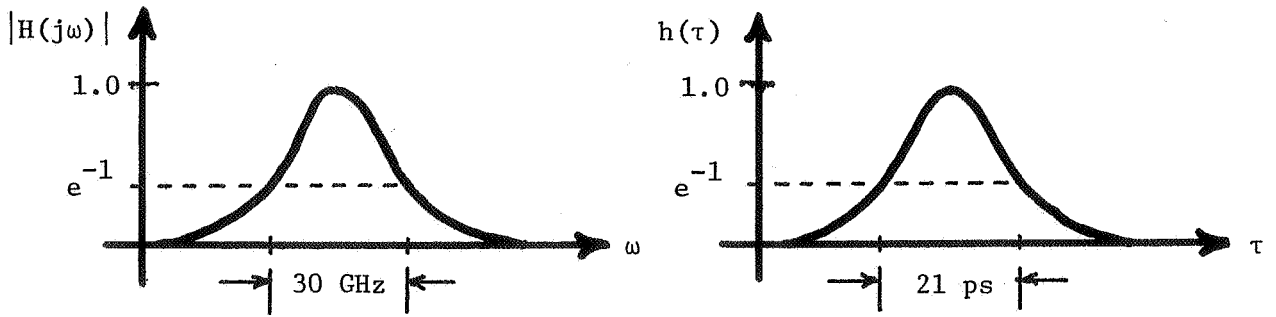


Figure 4.5. Gaussian system responses.

## 5. THE FREQUENCY DOMAIN SIX-PORT AUTOMATIC NETWORK ANALYZER

C. A. Hoer and C. M. Allred

### 5.1 Introduction

The six-port concept has been successfully applied in the realization of microwave reflectometers [5.1,5.2] and vector voltmeters [5.3]. A conventional six-port reflectometer is a six-port junction designed to measure reflection coefficient and power at one of its ports in terms of power readings taken at four of the other ports when an rf signal is applied at the remaining port. The measured or observed quantities are scalar as opposed to phasor quantities, i.e., the observables are ratios of transmitted power at the ports rather than complex voltages or currents. A typical realization of a six-port reflectometer is shown in figure 5.1 [5.4].

The value of the complex reflection coefficient  $\rho$  obtained from a six-port reflectometer is calculated from

$$\rho = \frac{\sum c_i P_i + j \sum s_i P_i}{\sum \alpha_i P_i} \quad (5.1)$$

which, with few exceptions, applies to any six-port junction [5.2]. The  $P_i$ 's are the power readings from four of the five detectors in figure 5.1a, where  $P_3$  must be one of the detectors used. The 12 real constants,  $c_i$ ,  $s_i$ , and  $\alpha_i$ , characterize the six port. They are functions only of the scattering parameters of the six port and of the reflection coefficient of the detectors. They are independent of the properties of the rest of the measurement system including the flexible cables and the generator. One can divide numerator and denominator of eq (5.1) by any one of these 12 constants leaving 11 new constants which must be determined by some calibration process such as those mentioned in section 5.3.

Using all five detectors, one can display approximate values of  $\rho$  on an oscilloscope as shown in figure 5.1b. This application is based on the following equation for this particular seven-port junction assuming ideal (i.e., lossless, infinite isolation, zero reflection, etc.) components [5.2]:

$$\rho = \frac{(P_5 - P_7) + j(P_6 - P_8)}{P_3} \quad (5.2)$$

As this equation shows,  $P_3$  acts like a scale factor.  $P_3$  can be measured to determine the scale of  $|\rho|$  on the oscilloscope screen. It can also be used to control the level of the generator. A real-time analog display of  $\rho$  is especially useful in checking out the measurement system.

By using two six-ports a network analyzer can be built which can be calibrated using a length of precision transmission line as the only standard needed. Two six-port reflectometers are used in the configuration shown in figure 5.2 to measure all the network parameters of any linear reciprocal or nonreciprocal, active or passive two-port, inserted between the two reflectometers. This configuration is most similar to the interference bridge described in 1962 by Altschuler [5.5]. The two measurement systems differ in that six-port reflectometers are used in place of slotted lines, isolators, and tuners. This change makes the present system easy to automate and broadband, in the sense that measurements can be made at any fixed frequency from 2 to 18 GHz after proper calibration at that frequency. Four-port reflectometers could be used in place of six-port reflectometers, but the system would not be as simple as the one described here. A great advantage of the six-port is that imperfect, and hence very broad band components, Q and D in figure 5.1, are used; all imperfections are accounted for in the calibration rather than tuned out at successive frequencies.

The measurement system described here differs from most other network analyzers in that the six-port reflectometers can be made small enough and portable enough to connect directly to the device under test, eliminating flexible cables or arms between the measurement system and the device being measured. Flexible cables "behind" each six port do not enter into the system calibration except in the measurement of the phase shift through nonreciprocal two ports. The present system is simpler than most other network analyzers in that no i-f source is used and no phase detectors are required.

Self-calibration techniques similar to those described by Allred and Manney [5.6] for calibrating two four-port couplers can be used to calibrate two six-port reflectometers. When applied to the dual six-port measurement system, this technique yields the constants in eq (5.1) needed to calculate  $\rho_1$  and  $\rho_2$ . Only one standard is required in the self-calibration technique. This standard can be a uniform length of transmission line or one known termination. Details of this self-calibration technique are given in references [5.7,5.8].

## 5.2 Theory of the Dual Six-Port Network Analyzer

### A. Determination of $S_{11}$ , $S_{22}$ , $|S_{12}|$ , $|S_{21}|$

The basic setup for using two six-port reflectometers to measure all of the scattering parameters of a two port is shown in figure 5.2. The rf signal is applied to both reflectometers simultaneously. Reflectometer 1 measures the complex ratio  $\rho_1 \equiv b_1/a_2$  at reference plane 1. Reflectometer 2 measures  $\rho_2 \equiv b_2/a_2$  at reference plane 2.  $\rho_1$  and  $\rho_2$  are not reflection coefficients in the normal sense, but simply relate two traveling waves in opposite directions. These two ratios are related by the S-parameters of the two port inserted between the two reflectometers. Let the scattering equations for the two port under test be

$$b_1 = S_{11}a_1 + S_{12}a_2 \quad (5.3)$$

$$b_2 = S_{21}a_1 + S_{22}a_2 \quad (5.4)$$

Dividing eq (5.3) by  $a_1$  and eq (5.4) by  $a_2$  gives

$$\rho_1 = \frac{b_1}{a_1} = S_{11} + S_{12} \frac{a_2}{a_1} \quad (5.5)$$

$$\rho_2 = \frac{b_2}{a_2} = S_{22} + S_{21} \frac{a_1}{a_2} \quad (5.6)$$

Since  $|a_2/a_1|$  can be greater or less than one,  $|\rho_1|$  and  $|\rho_2|$  can also be greater or less than one. Six-port reflectometers are capable of measuring values of  $|\rho|$  both larger and smaller than one.

Eliminating  $a_2/a_1$  from eqs (5.5) and (5.6) gives

$$(\rho_1 - S_{11})(\rho_2 - S_{22}) = S_{12}S_{21} \quad (5.7)$$

or

$$\rho_2 S_{11} + \rho_1 S_{22} - \Delta = \rho_1 \rho_2 \quad (5.8)$$

where  $\Delta$  is the determinant of the scattering matrix,

$$\Delta = S_{11}S_{22} - S_{12}S_{21} \quad (5.9)$$

Three equations like eq (5.8) are solved for  $S_{11}$ ,  $S_{22}$ , and  $\Delta$ . These equations are generated by measuring  $\rho_1$  and  $\rho_2$  for three different values of  $a_2/a_1$  which are determined by the setting of the attenuators  $A_1$  and  $A_2$  and of the phase shifter  $\phi$ . The values of  $A_1$ ,  $A_2$ , and  $\phi$  do not need to be known since they do not enter into the equations.

If it is known that the two port under test is reciprocal, so that  $S_{12} = S_{21}$ , the magnitude can be obtained from eq (5.9),

$$|S_{12}|^2 = |S_{21}|^2 = |S_{11}S_{22} - \Delta| \quad (5.10)$$

or from eq (5.7),

$$|S_{12}|^2 = |S_{21}|^2 = |(\rho_1 - S_{11})(\rho_2 - S_{22})|. \quad (5.11)$$

After three or more equations like eq (5.8) are solved for  $S_{11}$ ,  $S_{22}$ , and  $\Delta$ , then  $S_{11}$  and  $S_{22}$  can be used in eq (5.11) to calculate values of  $|S_{12}|$  and  $|S_{21}|$  for each measurement. The scatter in the values of  $|S_{12}|$  gives an indication of the precision with which  $|S_{12}|$  has been measured.

If it is not known that the two port under test is reciprocal,  $|S_{12}|$  and  $|S_{21}|$  are obtained from eqs (5.5) and (5.6) which give

$$|S_{12}| = |\rho_1 - S_{11}| \left| \frac{a_1}{a_2} \right| \quad (5.12)$$

$$|S_{21}| = |\rho_2 - S_{22}| \left| \frac{a_2}{a_1} \right|. \quad (5.13)$$

The six-port reflectometers can be used to measure  $|a_2/a_1|$  as well as  $\rho_1$  and  $\rho_2$  in these equations. Altschuler [5.4] discusses the advantages of making  $|a_2/a_1|$  large or small to increase the sensitivity when measuring small values of  $S_{12}$  or  $S_{21}$ .

#### B. Determination of $\psi_{12} = \psi_{21}$

The equations given in sections 5.2A can be used to determine all of the scattering parameters except  $\psi_{12}$  and  $\psi_{21}$ , the phase angles of  $S_{12}$  and  $S_{21}$ . For either a reciprocal or nonreciprocal two port, eqs (5.5) and (5.6) give

$$\psi_{12} = \psi_1 - \psi_a \quad (5.14)$$

$$\psi_{21} = \psi_2 + \psi_a \quad (5.15)$$

where

$$\psi_1 \equiv \arg(\rho_1 - S_{11}) \quad (5.16)$$

$$\psi_2 \equiv \arg(\rho_2 - S_{22}) \quad (5.17)$$

$$\psi_a \equiv \arg(a_2/a_1). \quad (5.18)$$

Since the six-port reflectometers do not directly measure the phase angle of  $a_2/a_1$ , the angle  $\psi_a$  is not yet known. The angles  $\psi_1$  and  $\psi_2$  are known from measured values of  $\rho_1$  and  $\rho_2$  and computed values of  $S_{11}$  and  $S_{22}$  (see sec. 5.2A).

When the two port is reciprocal, eqs (5.14) and (5.15) can be solved for both  $\psi_a$  and  $\psi_{12} = \psi_{21}$ ;

$$\psi_{12} = \psi_{21} = \frac{\psi_1 + \psi_2}{2} + n\pi, \quad n = 0, 1 \quad (5.19)$$

$$\psi_a = \frac{\psi_1 - \psi_2}{2} + n\pi, \quad n = 0, 1 \quad (5.20)$$

where the ambiguity  $n\pi$  arises from the division by 2, and  $n$  is an integer. All phase angles considered here are modulo  $2\pi$  as in any frequency domain measurements. It can be seen from eqs (5.14) and (5.15) that  $n$  must take on the same value in eqs (5.19) and (5.20). The value of  $n$  can be determined from either an estimate of  $\psi_{12}$  or  $\psi_a$ . A good estimate of  $\psi_a$  can be obtained from equations derived for the nonreciprocal case which is considered in section 5.2C.

The measurement technique described up to this point is similar to methods which use only one reflectometer to measure  $\rho_1$  when the two port is terminated with three different known terminations at reference plane 2. The equations which apply when using known terminations are the same as eqs (5.3) to (5.20) if  $\rho_2$  is replaced by  $1/\Gamma_L$  where  $\Gamma_L$  is the reflection coefficient of the termination at reference plane 2. The difference here is that  $a_2$  can be made much larger than if passive terminations are used. This makes it possible to measure larger values of attenuation using the setup in figure 5.2. Another difference is that the ratio  $|a_2/a_1|$  cannot be measured when passive terminations are used so that  $S_{12}$  and  $S_{21}$  of nonreciprocal two ports cannot be measured.

### C. Determination of $\psi_{12} \neq \psi_{21}$

When the two port under test is not reciprocal,  $\psi_{12}$  and  $\psi_{21}$  must be calculated from eqs (5.14) and (5.15) where  $\psi_a$  can be determined as follows. The determination of  $\psi_a$  depends in part on knowledge of the measurement system which can be viewed as a three-port junction whose ports are 1, 2, and 3 (near the generator) in figure 5.2. For this three-port junction, one can show that

$$\frac{a_2}{a_1} = \left( s_{21} - s_{11} \frac{s_{23}}{s_{13}} \right) \rho_1 - \left( s_{12} \frac{s_{23}}{s_{13}} - s_{22} \right) \rho_2 \frac{a_2}{a_1} + \frac{s_{23}}{s_{13}} \quad (5.21)$$

where the small  $s_{ij}$ 's are the scattering parameters of the equivalent three-port measurement system. Rewrite eq (5.21) as

$$\frac{a_2}{a_1} = C_1 \rho_1 - C_2 \left( \rho \frac{a_2}{a_1} \right) + C_3 \quad (5.22)$$

where  $C_1$ ,  $C_2$ , and  $C_3$  are defined by corresponding terms in eqs (5.21) and 5.22). The  $C$ 's for a particular setting of  $A_1$ ,  $A_2$ , and  $\phi$  can be determined from three equations like eq (5.22) when  $\rho_1$ ,  $\rho_2$ , and  $a_2/a_1$  are known, which is the case when reciprocal two ports are measured. solving eq (5.22) for  $a_2/a_1$ ,

$$\frac{a_2}{a_1} = \frac{C_3 + C_1 \rho_1}{1 + C_2 \rho_2} \quad (5.23)$$

Once the  $C$ 's are known,  $\psi_a$  can be calculated from eq (5.23) when measuring either reciprocal or nonreciprocal two ports.

When the two port is nonreciprocal,  $\psi_a$  calculated from eq (5.23) is used in eqs (5.14 and (5.15) to calculate  $\psi_{12}$  and  $\psi_{21}$ . When the two port is reciprocal, the value of  $\psi_a$  from eq (5.23) is considered to be only an estimate for determining  $n$  in eq (5.20). This is because the value of  $\psi_a$  calculated from eq (5.20) will, in general, be more accurate than that calculated from eq (5.23). Since the C's in eq (5.23) are functions of the scattering parameters of the three-port measurement system, they are functions of the stability of the flexible cables and also of the setting and repeatability of the components  $A_1$ ,  $A_2$ , and  $\phi$ . None of the other equations up to eq (5.21) are functions of these components or the cables. For this reason, eq (5.23) is used only to calculate  $\psi_a$  and not  $|a_2/a_1|$  which can be obtained from the two six-port reflectometers independently of the properties of the three-port measurement system. Then all of the calculated S-parameters of the two port under test will be independent of the properties of the three-port measurement system except  $\psi_{12}$  and  $\psi_{21}$  of nonreciprocal two ports.

### 5.3 Using Six-Port Systems for $\mu$ - $\epsilon$ Measurements

#### 5.3.1 The Six-Port Reflectometer

One way of measuring the magnetic and dielectric properties of small samples at fixed frequencies is with a six-port reflectometer (fig. 5.3). A six-port reflectometer is a six-port junction such as shown in figure 5.1 designed to measure reflection coefficient and power at one of its ports in terms of power readings taken at four of the other ports when an rf signal is applied at the remaining port. The complex reflection coefficient,  $\Gamma$ , is given in terms of the four power readings,  $P_3 \dots P_6$ , by eq (5.1) or more compactly by

$$\Gamma = \frac{\sum z_i P_i}{\sum \alpha_i P_i}, \quad i = 3, 4, 5, 6, \quad (5.24)$$

where the four complex constants  $z_i$  and the four real constants  $\alpha_i$  are functions of the six-port junction. These constants are obtained by a calibration process involving at least one but usually more known terminations which are connected to the measurement port. The properties of a sample can be obtained from measurements of  $\Gamma$  with and without the sample in the holder.

The main advantage of the six-port reflectometer over the conventional four-port reflectometer is that the phase angle as well as magnitude of  $\Gamma$  is obtained from simple power measurements. It is not necessary to have a phase detector on the sidearm of the six port to measure the phase of  $\Gamma$ . Only one source is used since no frequency conversion is involved. The six port is relatively easy to automate since all information is obtained from a set of dc voltage readings taken from the four power meters.

The resolution in measuring  $\Gamma$  is essentially the resolution in measuring the four values of power which is one part in  $10^4$  for thermistor types of power detectors. These detectors are commercially available up to 100 GHz. Waveguide components for constructing six-port junctions are also commercially available to 100 GHz. Therefore it should be possible to construct six-port reflectometers in each waveguide band up to 100 GHz and possibly even higher.

An experimental automated waveguide six-port reflectometer has been constructed at NBS for measurement of power and  $\Gamma$  in the 50 to 75 GHz range. Preliminary data indicate that it has a resolution of 0.0001 in measuring  $\Gamma$  in this frequency range. The accuracy has not yet been determined, but for small changes in  $\Gamma$  ( $\Delta \Gamma < 0.1$ ), the accuracy of the change is expected to be limited primarily by the resolution. The time required to measure  $\Gamma$  is several seconds per frequency. Most of that time is required to set and phase-lock the frequency. This time can be reduced considerably by not locking the frequency, but the accuracy would be decreased.

#### 5.3.2 The Dual Six-Port Network Analyzer

Another way of measuring the properties of a sample is to insert it in a two-port sample holder which is inserted between two six-port reflectometers as shown in figure 5.4. The two six-port reflectometers are capable of measuring all of the scattering parameters of the two port with and without the sample inserted in the holder. These measurements should yield both the transmission and reflection properties of the sample.

There are several advantages in having two six-port reflectometers instead of one. It is much easier to calibrate two six-port reflectometers than it is to calibrate just one in that fewer connections need to be made by the operator, and fewer standards are required. The only standards needed to calibrate a pair of six ports are a flat short and a length of precision waveguide. A typical calibration procedure is outlined in figure 5.5

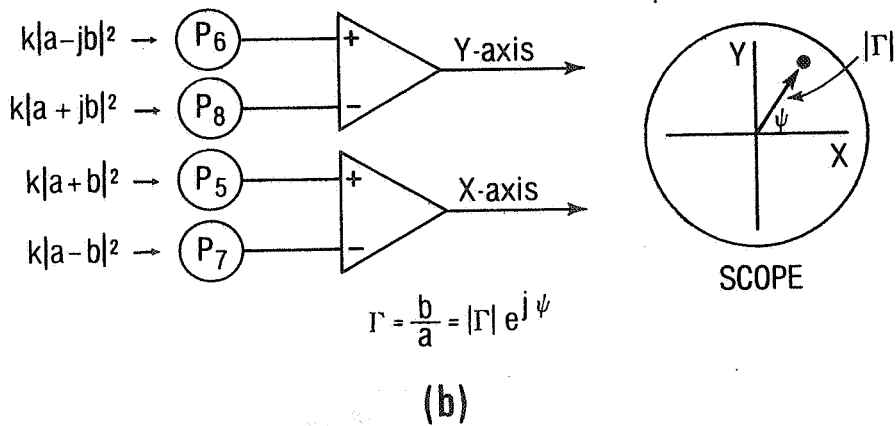
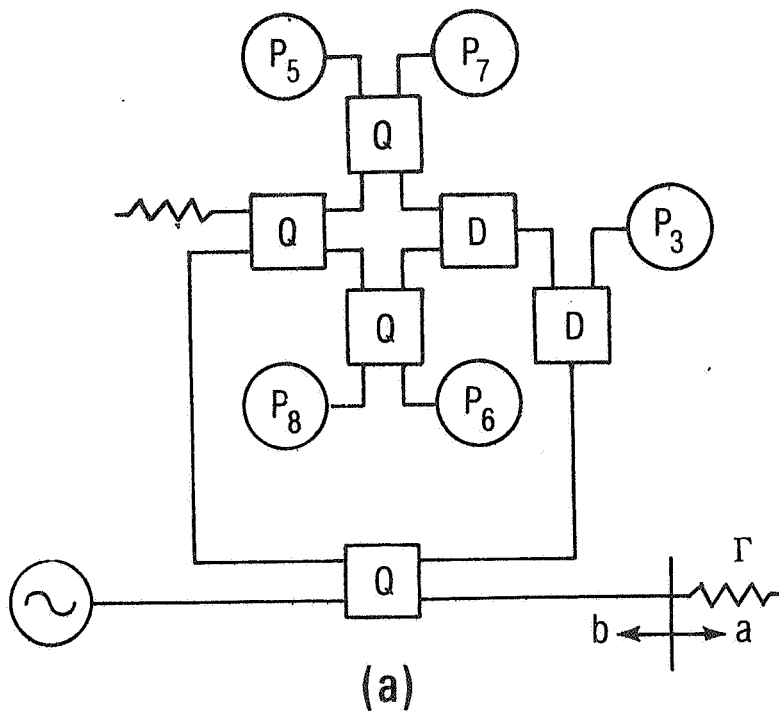
Another advantage is that by connecting the two six-port measurement ports together, one can determine if the two reflectometer measurements of  $\Gamma$  agree with each other. The stability of the calibration with time can thus be determined and monitored.

A pair of coaxial six-port reflectometers have been constructed at NBS for measuring S-parameters of two-port devices in the range of 2 to 18 GHz. The techniques and software for calibrating this pair of reflectometers should be applicable to waveguide systems at higher frequencies. The precision of the NBS dual six-port system in measuring the S-parameters of a two port is approximately 0.0001.

One disadvantage in measuring all of the S-parameters is that it takes about eight times as long as it does to measure  $\Gamma$  with a single six port.

#### 5.4 References

- [5.1] Engen, G. F., The six-port reflectometer: An alternative network analyzer, IEEE Trans. on Microwave Theory and Tech. MTT-25, No. 12, 1075-1080 (Dec. 1977).
- [5.2] Hoer, C. A., Using six-port and eight-port junctions to measure active and passive circuit parameters, NBS Tech. Note 673, Nat. Bur. Stand., Boulder, CO (Sept. 1975).
- [5.3] Hoer, C. A. and K. C. Roe, Using an arbitrary six-port junction to measure complex voltage ratios, IEEE Trans. Microwave Theory and Tech. MTT-23, 978-984 (Dec. 1975).
- [5.4] Hoer, C. A., A network analyzer incorporating two six-port reflectometers, IEEE Trans. on Microwave Theory and Tech. MTT-25, No. 12, 1070-1074 (Dec. 1977).
- [5.5] Altschuler, H. M., The measurement of arbitrary linear microwave two ports, Proc. Inst. Elec. Eng. 109, Pt. B, Supple. No. 23, 704-712 (May 1962).
- [5.6] Allred, C. M., and Manney, C. H., The calibration and use of directional couplers without standards, IEEE Trans. Instr. Meas. IM-25, 84-89 (March 1976).
- [5.7] Hoer, C. A., Calibrating two six-port reflectometers, NBS Tech. Note 1004, Nat. Bur. Stand., Boulder, CO (June 1978).
- [5.8] Engen, G. F., Hoer, C. A., Speciale, R. A., The application of "thru-short-delay" to the calibration of the dual six port, 1978 IEEE MTT-S International Microwave Symposium Digest, 184-185 (June 1978).



A seven-port reflectometer constructed with quadrature hybrids Q, and in-phase power dividers D, in a conventional circuit to measure reflection coefficient  $\Gamma$ . A six-port reflectometer is obtained by simply ignoring one of the four outputs  $P_3 \dots P_8$ . If the detectors each have an output dc voltage proportional to the input RF power, the voltages can be applied to an oscilloscope as in (b) to get a display of reflection coefficient  $\Gamma$ . The constant  $k$  need not be known to display  $\Gamma$ . When the termination is replaced with a two port, the ratio  $p$  is displayed instead of  $\Gamma$ .

Figure 5.1. A six-port reflectometer.

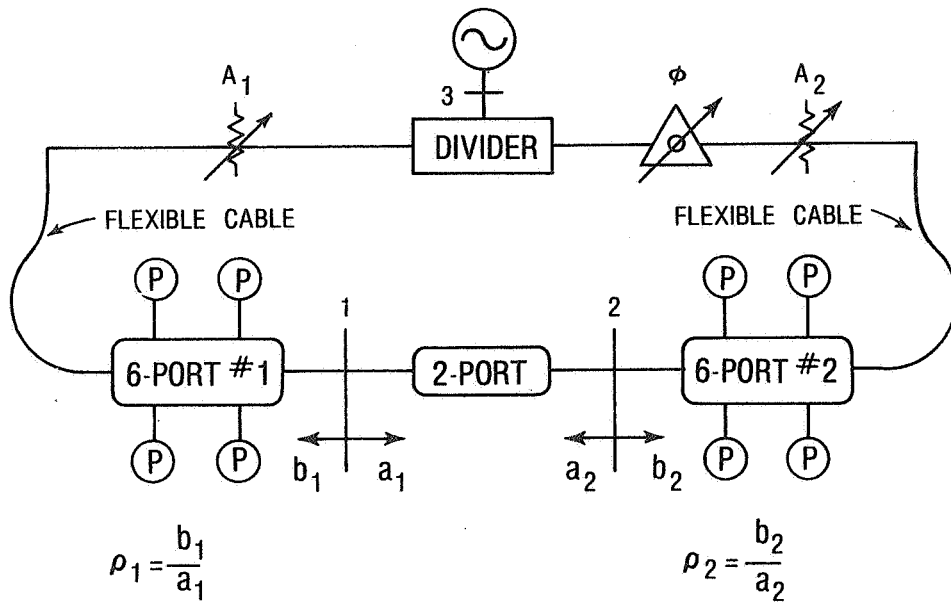


Figure 5.2. Basic circuit for measuring all of the scattering parameters of a two port with two six-port reflectometers.

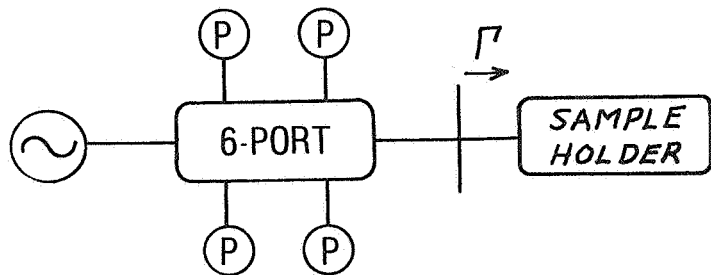


Figure 5.3. Six-port reflectometer  $\mu$ - $\epsilon$  measurement system.

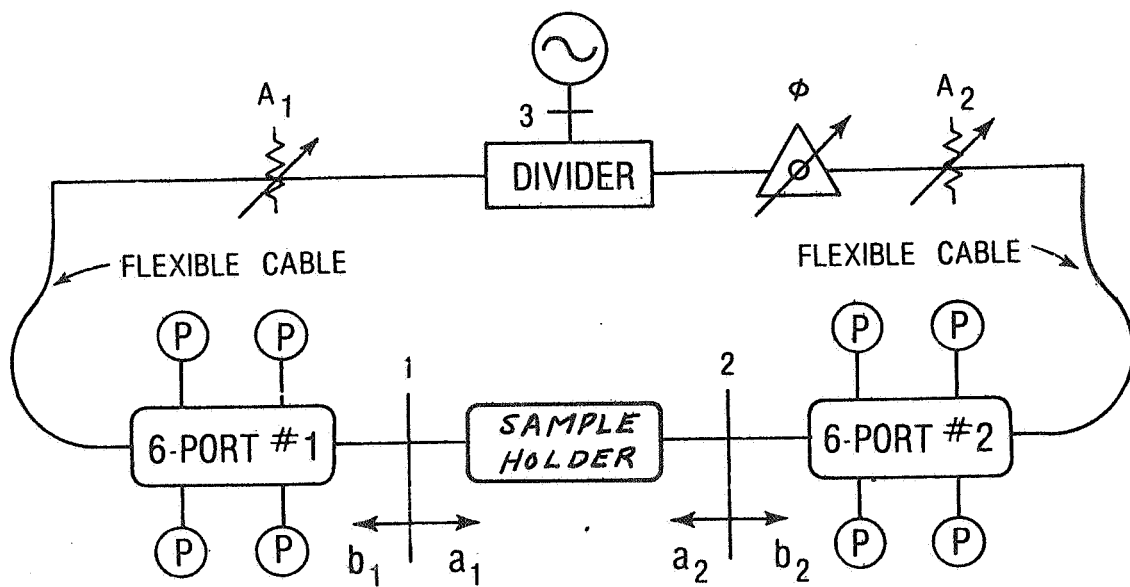
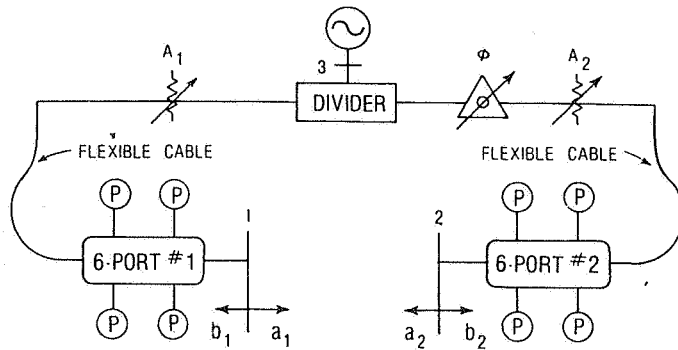


Figure 5.4. The dual six-port network  $\mu$ - $\epsilon$  measurement system.

DUAL 6-PORT ANA



"6-PORT TSD" CALIBRATION TECHNIQUE

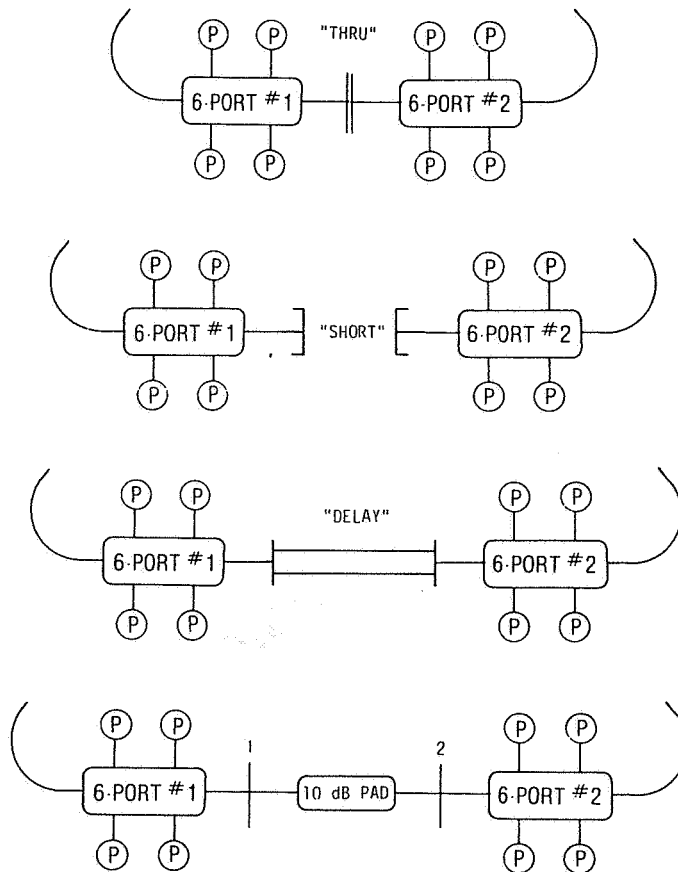


Figure 5.5. The four different connections made in calibrating the dual 6-port ANA with the "6-port TSD" technique, where TSD stands for "Thru", "Short", "Delay". The parameters of the normal 10 dB pad do not need to be known.

## 6. CONCLUSION

### 6.1 Summary

The purpose of this report was to describe new methods for implementing automatic  $\mu$ - $\epsilon$  measurements of radar absorber materials for applications primarily above 20 GHz. After reviewing the literature and drawing upon the collective experience of the NBS staff, three methods were selected for discussion:

1. The Time Domain Automatic Network Analyzer.
2. Correlation Measurement Systems Using Noise Signal Sources.
3. The Six-Port Frequency Domain Automatic Network Analyzer.

Because there were several technical options in implementing a time domain automatic network analyzer, consideration had to be given to four topics:

- a) Extension of present baseband system performance to higher frequencies.
- b) Millimeter wave pulse generators.
- c) Heterodyne techniques.
- d) Improvement of picosecond-domain sampling heads.

For each of the three new methods discussed in this report, related time domain, correlation and microwave research and development have been implemented at NBS in the past for other applications. Consequently, all three methods are feasible.

### 6.2 Discussion

The central question to be addressed is simply, "which method or methods would achieve the most effective results?"

There are two important factors to consider in answering the question. The first is the time and effort required to refine the method(s) for application above 20 GHz and into the millimeter wave region to about 100 GHz. The second factor depends upon the sample-holder structure.

In the technical descriptions presented in Chapters 2, 4, and 5, it was assumed that the sample fits exactly within the system waveguide, i.e., the sample holder was a uniform piece of waveguide which was completely filled by the sample, and the sample faces were plane and parallel to the wavefront of the principal waveguide mode. These assumptions become increasingly difficult to satisfy when: (1) waveguide dimensions are decreased to allow only principal mode propagation, and (2) the sample physical properties are such that the sample is difficult to shape and susceptible to damage which can alter its electromagnetic and/or physical properties. Consequently, these assumptions become increasingly untenable with increasing frequency. The only alternative available is to depart from the principal mode sample holder and employ an electromagnetically large or over-moded sample holder.

Physically large sample holders could approach free-space conditions in which the sample is placed between two antennas and irradiated by a characterized wavefront emanating from one of the antennas. The wavefront passes through the sample and is received by the second antenna. However, such a system would ideally require a very large sample, i.e., a large, thin, plane sheet.

In practice, available samples are 10 to 15 cm (4 to 6 inches) square. Consequently, if such samples are to be directly used without physical alteration, the sample holder would have to be one which would accept the whole sample and provide a characterizable electromagnetic coupling to the sample. Clearly, the sample holder would be over-moded and for the higher frequencies approach a quasi free-space condition. The critical factor which must be resolved for a successful application of an over-moded or quasi free-space sample holder is the characterization of the electromagnetic coupling to the sample. If the coupling is known, then transmission and/or reflection data can be analyzed to yield the electromagnetic parameters  $\mu$  and  $\epsilon$ .

It is important to recognize that both the time domain and frequency domain  $\mu$  and  $\epsilon$  measurement methods require characterization of the over-moded electromagnetic coupling to the sample. Consequently, this means that the network properties or physical model must be determined to establish the transfer functions between the uniform waveguide reference planes and the sample. Neither the frequency domain nor the time domain approach eliminates the need to establish the transfer functions of the over-moded or quasi free-space sample holder.

### 6.3 Recommendations

In answer to the central question stated at the beginning of section 6.2, it is recommended that future work include the following technical approaches:

1. Heterodyne Time Domain Automatic Network Analyzer.
2. Six-Port Automatic Network Analyzer.
3. Over-moded sample holders.

The first two approaches primarily require a development effort utilizing available microwave or millimeter wave components and available mini-computer systems and interfaces. The third approach requires a research effort to establish the properties of over-moded or quasi free-space sample holders.

U.S. DEPT. OF COMM. BIBLIOGRAPHIC DATA SHEET	1. PUBLICATION OR REPORT NO.  NBSIR 79-1613		3. Recipient's Accession No.
4. TITLE AND SUBTITLE  RADAR ABSORBER MEASUREMENT TECHNIQUES AT FREQUENCIES ABOVE 20 GHz		5. Publication Date August 1979	
7. AUTHOR(S) N. S. Nahman, C. M. Allred, J. R. Andrews, C. A. Hoer and R. A. Lawton		8. Performing Organ. Report No.	
9. PERFORMING ORGANIZATION NAME AND ADDRESS  NATIONAL BUREAU OF STANDARDS DEPARTMENT OF COMMERCE WASHINGTON, DC 20234		10. Project/Task/Work Unit No. 7244440	
12. SPONSORING ORGANIZATION NAME AND COMPLETE ADDRESS (Street, City, State, ZIP) Department of the Air Force Air Force Avionics Laboratory (AFSC) Wright-Patterson Air Force Base, Ohio 45433		11. Contract/Grant No.	
15. SUPPLEMENTARY NOTES  <input type="checkbox"/> Document describes a computer program; SF-185, FIPS Software Summary, is attached.		13. Type of Report & Period Covered	
16. ABSTRACT (A 200-word or less factual summary of most significant information. If document includes a significant bibliography or literature survey, mention it here.)  New methods for implementing automatic permittivity/permeability measurements of radar absorber materials for applications primarily above 20 GHz and into the millimeter wave region to about 100 GHz are discussed. A brief review of the state-of-the-art of dielectric and magnetic material measurements is given. Automated time domain and frequency domain methods are considered including time domain automatic network analyzers, correlation measurement systems using noise signal sources, and six-port network analyzers.		14. Sponsoring Agency Code	
17. KEY WORDS (six to twelve entries; alphabetical order; capitalize only the first letter of the first key word unless a proper name; separated by semicolons)			
Dielectrics; Frequency-domain measurements; Magnetic materials; Microwaves; Millimeter waves; Permeability measurements; Permittivity measurements; Radar absorbers; Time-domain Measurements			
18. AVAILABILITY  <input checked="" type="checkbox"/> Unlimited  <input type="checkbox"/> For Official Distribution. Do Not Release to NTIS  <input type="checkbox"/> Order From Sup. of Doc., U.S. Government Printing Office, Washington, DC 20402, SD Stock No. SN003-003-  <input checked="" type="checkbox"/> Order From National Technical Information Service (NTIS), Springfield, VA. 22161	19. SECURITY CLASS (THIS REPORT)  UNCLASSIFIED	21. NO. OF PRINTED PAGES  72	
	20. SECURITY CLASS (THIS PAGE)  UNCLASSIFIED	22. Price  \$4.50	